LIST OF PUBLICATIONS

PUBLICATIONS (Thesis)

- **Patel, S**., Jana, S., Chetty, R., Thakore, S., Singh, M., & Devkar, R. (2017). **Toxicity evaluation of magnetic iron oxide nanoparticles reveals neuronal loss in chicken embryo**. *Drug and chemical toxicology*, 1-8.
- **Patel, S**., Jana, S., Chetty, R., Thakore, S., Singh, M., & Devkar, R., **TiO_2 nanoparticles induce omphalocele in chicken embryo by disrupting Wnt signaling pathway** (Manuscript submitted).

PUBLICATIONS (Collaboration)

- Jana, Sarmita, Dipak Patel, **Shweta Patel**, Kapil Upadhyay, Jaymesh Thadani, Rahul Mandal, Santasabuj Das, and Ranjitsinh Devkar. "Anthocyanin rich extract of Brassica oleracea L. alleviates experimentally induced myocardial infarction." *PloS one* 12, no. 8 (2017): e0182137.
- Solanki, Ankita, Mehul H. Sadhu, **Shweta Patel**, Ranjitsinh Devkar, and Sujit Baran Kumar. "Ternary complexes of copper (II) and cobalt (II) carboxylate with pyrazole based ligand: Syntheses, characterization, structures and bioactivities." *Polyhedron* 102 (2015): 267-275.
- Sharma, Radhika, Shubhangi S. Soman, **Shweta V. Patel**, and Ranjitsinh V. Devkar. "Studies in the synthesis and applications of 4-(aminomethyl) quinolin-2 (1H)-one derivatives as anti-cancer agents.

SCIENTIFIC REPORTS

OPEN

TiO_2 nanoparticles induce omphalocele in chicken embryo by disrupting Wnt signaling pathway

Received: 8 December 2017
Accepted: 5 March 2018
Published online: 19 March 2018

Shweta Patel[1], Sarmita Jana[1], Rajlakshmi Chetty[3], Sonal Thakore[2], Man Singh[3] & Ranjitsinh Devkar[1]

Titanium dioxide nanoparticles (TiO_2 NPs) are among abundantly used metal oxide NPs but their interactions with biomolecules and subsequent embryonic toxicity in higher vertebrates is not extensively reported. Physicochemical interactions of TiO_2 NPs with egg albumen reveals that lower doses of TiO_2 NPs (10 and 25 µg/ml) accounted for higher friccohesity and activation energy but an increment in molecular radii was recorded at higher doses (50 and 100 µg/ml). FTIR analysis revealed conformational changes in secondary structure of egg albumen as a result of electrostatic interactions between egg albumen and TiO_2 NPs. The morphometric data of chicken embryo recorded a reduction at all the doses of TiO_2 NPs, but toxicity and developmental deformity (omphalocele and flexed limbs) were recorded at lower doses only. Inductively coupled plasma optical emission spectrometry (ICP-OES) confirmed presence of Ti in chicken embryos. mRNA levels of genes involved in canonical and non-canonical Wnt signaling were lowered following TiO_2 NPs treatment resulting in free radical mediated disruption of lateral plate mesoderm and somite myogenesis. Conformational changes in egg albumen and subsequent developmental deformity in chicken embryo following TiO_2 NPs treatment warrants detailed studies of NP toxicity at lower doses prior to their biomedical applications.

Nanotechnology is a rapidly expanding field, with a wide range of applications in communications, robotics, medicine, clothes, sporting goods, etc[1,2]. According to a recent survey, the number of nanotechnology-based consumer products available in the world market is more than 1800[3]. The increased use of nanomaterials is also under scrutiny due to their adverse effects on the environment, physiology and overall survival of organisms. Titanium dioxide nanoparticles (TiO_2 NPs) are the most abundantly used nano metal oxides with their documented industrial uses in pigments and additives for paints, paper, ceramics, plastics, foods, and other products. The estimated worldwide production of TiO_2 NPs is 10000 tons/year for 2011–2014 and 2.5 million metric tons/year by 2025[4]. Therefore, risk assessment studies have predicted that TiO_2 NPs will be the most prevalent nanomaterials in environment[5].

Cytotoxic potential of TiO_2 NPs is well documented in a variety of cell lines. Oxidative DNA damage and apoptosis in HepG2 cells and in human epidermal cells[6], apoptosis and/or necrosis in human astrocytoma (astrocytes-like) U87 cells[7] and mitochondrial dysfunction in BRL 3A cells[8] are some of the recent reports on cytotoxicity of TiO_2 NPs. Toxicity of TiO_2 NPs based on difference in their size has been documented in nematodes[9] and earthworm[10]. The ability of TiO_2 NPs to produce reactive oxygen species and surface charge are the reasons accredited for their toxicity[6,11]. Several engineered nanometals including TiO_2 NPs have been known to persist in the food chain and move across trophic levels resulting in various forms of toxic manifestations[11]. Hence, their effect on reproductive performance and embryonic development cannot be ignored. Accelerated hatching of larvae and deformed embryos in zebrafish[12] and histopathological changes in juvenile carp[13] are few evidences on TiO_2 NPs induced toxicity on embryonic and post-hatch development. Hatching inhibition and malformation of embryos of Abalone have been reported following TiO_2 NPs exposure[14]. Also, prenatal exposure of TiO_2 NPs in female rats impacts genes controlling brain development in offspring[15] providing compelling evidences on systemic and developmental toxicity.

[1]Department of Zoology, Faculty of Science, The M.S. University of Baroda, Vadodara, India. [2]Department of Chemistry, Faculty of Science, The M.S. University of Baroda, Vadodara, India. [3]School of Chemical sciences, Central University of Gujarat, Gandhinagar, India. Correspondence and requests for materials should be addressed to R.D. (email: rv.devkar-zoo@msubaroda.ac.in)

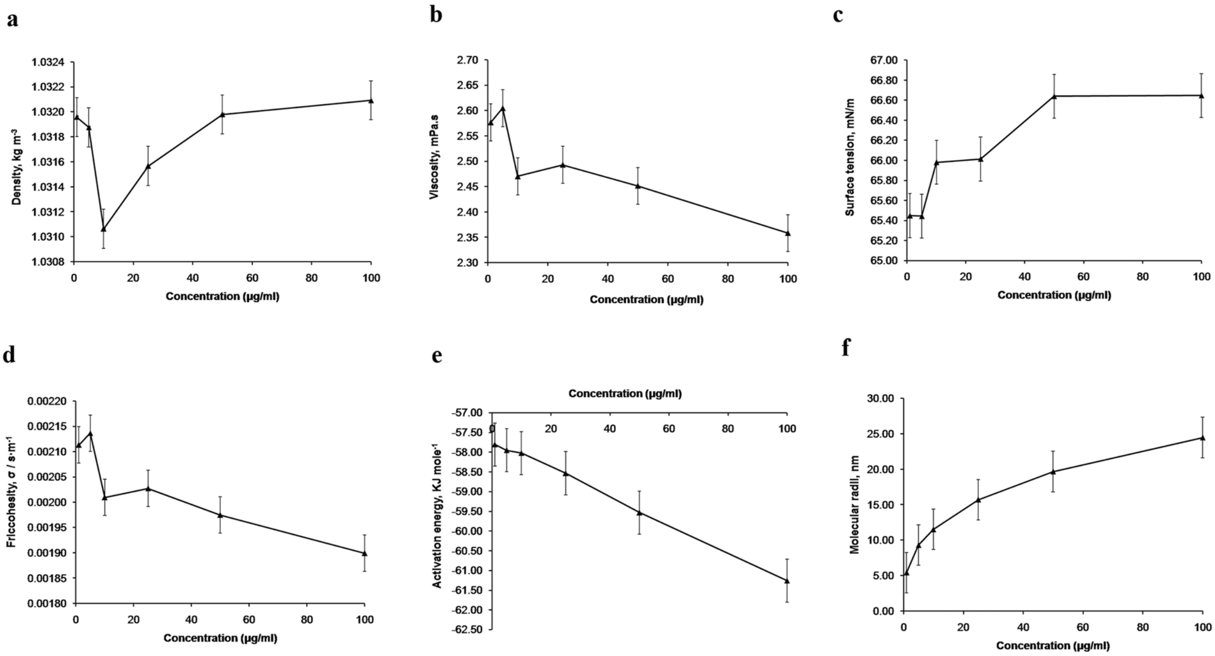

Figure 1. Physicochemical analysis of titanium dioxide nanoparticles and their interaction with egg albumen. Density, Viscosity, Surface tension, Friccohesity, Activation energy and Molecular radii of TiO_2 NPs in albumen (**a**–**f**) respectively.

Chicken embryo is a sensitive and popularly used model for assessing developmental toxicity and teratogeny of various nanoparticles. Hence, chicken embryo was chosen as an experimental model in our study to assess the impact of TiO_2 NPs on embryonic development. Other studies had reported developmental toxicity of graphite[16], copper[17], carbon[18], platinum[19], pristine graphene[20] and silver[21] nanoparticles on chicken embryo, but their *in ovo* physicochemical interactions with biomolecules such as egg albumen have not been taken into account. In the present study, we assess the interaction of TiO_2 NPs with egg albumen and its subsequent impact on chicken embryonic development.

Results

In DLS analysis, TiO_2 NPs presented a single distribution with peak centered at 88.6 nm. The plot showed that the nanoparticles have a narrow size distribution with an average diameter of about 88.6 nm (Supplementary Figure S1).

Physicochemical analysis. Results shown herein are quantification of interaction of peptide bonds with TiO_2 NPs and alteration in the Lennard Jone potential that varies spontaneity and strength of interactive force. There was a decrement in density (1.031064 kg.m^{-3}) of TiO_2 NPs + albumen at 10 μg/ml, whereas, 25, 50 and 100 μg/ml recorded steadily ascending values (1.031567, 1.031979 and 1.032092 kg.m^{-3} respectively) (Fig. 1a and Supplementary Table S2). Lower concentrations of TiO_2 NPs (1 and 5 μg/ml) recorded higher viscosity indices (2.57 and 2.60 mPa.s). The viscosity indices of 10, 25 and 50 μg/ml doses were comparable to each other (2.47, 2.49 and 2.45 mPa.s) but, 100 μg/ml dose accounted for a decline in viscosity (2.35 mPa.s) (Fig. 1b and Supplementary Table S2). Indices of surface tension showed an increase at 10 μg/ml concentration of TiO_2 NPs (65.98 mN.m^{-1}) as compared to 1 and 5 μg/ml concentrations (65.45 and 65.44 mN.m^{-1} respectively). However, 25, 50 and 100 μg/ml doses recorded a steady increment in surface tension (66.01, 66.64 and 66.65 mN.m^{-1}) (Fig. 1c and Supplementary Table S2). Friccohesity indices showed a decline at 10 μg/ml TiO_2 NPs (0.002009 s.m^{-1}) as compared to 1 and 5 μg/ml concentrations (0.002113 and 0.002136 s.m^{-1} respectively). A steady decline in friccohesity (0.002027, 0.001974 and 0.001899 s.m^{-1} at 25, 50 and 100 μg/ml doses respectively) was also observed in this study (Fig. 1d and Supplementary Table S2). A dose dependent decline in activation energy was recorded from 1–100 μg/ml doses with −57.81 KJ.mole^{-1} as the highest value and −61.26 KJ.mole^{-1} as the lowest value respectively (Fig. 1e and Supplementary Table S2). An increase in molecular radii (5–11.53 nm) was observed at 1–10 μg/ml TiO_2 NPs. Further, a steady increase in molecular radii (15.69, 19.66 and 24.45 nm) was observed at 25, 50 and 100 μg/ml doses respectively (Fig. 1f and Supplementary Table S2).

Spectroscopic characterization. Comparative FTIR spectra (400–4000 cm^{-1}) of native albumen and TiO_2 NPs + albumen depicting amide A (around 3400 cm^{-1}), amide B (about 3090 cm^{-1}), amide I and II (region between 1600–1700 cm^{-1}) domains are shown in Fig. 2a. The broad peak at 3591 and 3434 cm^{-1} in the amide A region of native albumen corresponds to the H-O-H asymmetric and symmetric stretching respectively whereas TiO_2 NPs + albumen recorded a shift in H-O-H stretching peak to 3478 cm^{-1}. Also, a shift in peak from 2071 cm^{-1} (in albumen) to 2083 cm^{-1} (TiO_2 NPs + albumen) was recorded. The amide I and II secondary

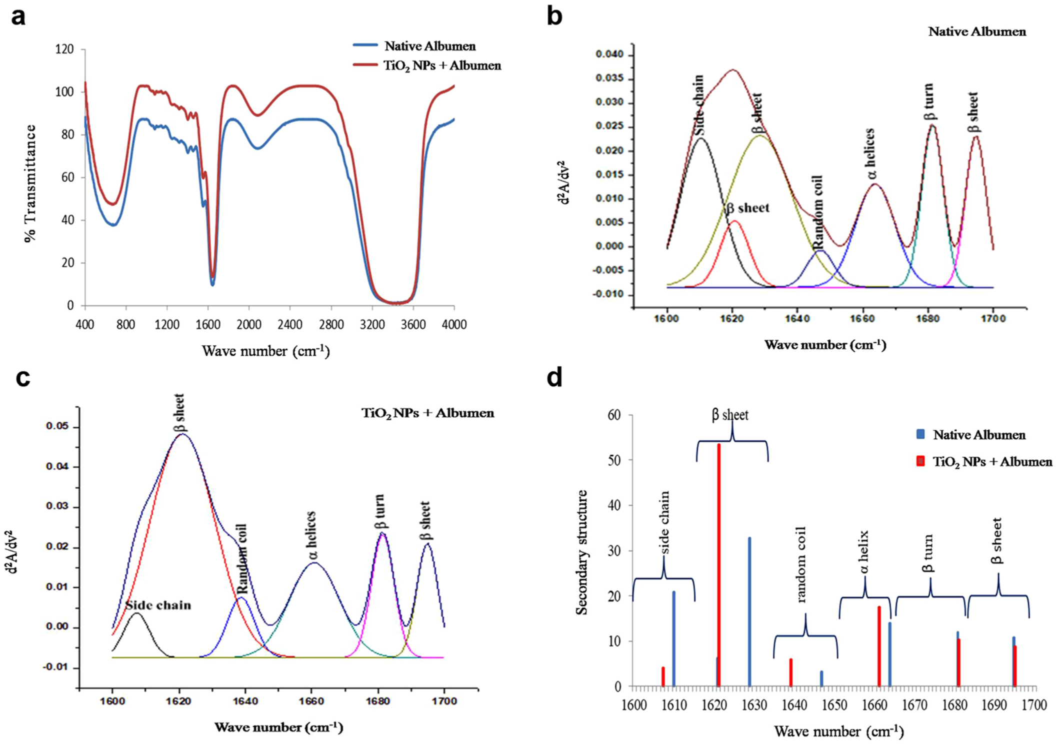

Figure 2. FTIR spectra of native egg albumen and TiO_2 NPs + Albumen. (**a**) Entire spectral range from 400–4000 cm^{-1}; (**b**–**d**) Gaussian curve fitting of secondary derivative of Native Albumen and TiO_2 NPs + Albumen with Comparative Secondary structure elements from FTIR spectra.

fingerprint regions (in albumen) recorded two peaks at 1651 cm^{-1} and 1642 cm^{-1} but in TiO_2 NPs + albumen a peak was recorded at 1641 cm^{-1}. A peak in the amide III region was recorded at 1243 cm^{-1} in albumen whereas, TiO_2 NPs + albumen recorded a shift to peak 1551 cm^{-1}. Also, peaks at 1457 and 1451 cm^{-1} in albumen and TiO_2 NPs + albumen respectively are due to $-CH_2$ scissoring vibration whereas, a peak at 675 cm^{-1} in TiO_2 NPs + albumen corresponds to Ti-O vibrational mode of TiO_2 NPs. Results obtained in deconvoluted Gaussian fitted spectra (Fig. 2b,c) and integrated peak areas of secondary-derivative structure element (Fig. 2d and Supplementary Table S3) and in albumen and TiO_2 NPs + albumen showed that albumen was mainly composed of side chain (1610 cm^{-1}, 20.93%) inter or intramolecular β sheet (1621–1629 cm^{-1}, 39.11%) closely followed by α helices (1664 cm^{-1}, 13.94%) with minor proportions of β turns (1681 cm^{-1}, 11.95%) and β sheet (1695 cm^{-1}, 10.76%). After interaction with TiO_2 NPs, a decrease in side chain (1607 cm^{-1}, 4.11%), β turns (1681 cm^{-1}, 10.31%) and β sheet (1695 cm^{-1}, 8.81%) and an increase in inter or intramolecular β sheet (1621 cm^{-1}, 53.39%) and α helices (1661 cm^{-1}, 17.46%) was recorded.

Natality and Morphometry of Chick embryos. Lower doses (10 and 25 μg/ml) of TiO_2 NPs treatment accounted for 12.5% and 25% viable embryos respectively on 19^{th} day of incubation. Also, 56.25% and 43.75% embryos were found to be malformed at 10 and 25 μg/ml doses. However, higher doses (50 and 100 μg/ml) recorded viable embryos ranging between 75–87.5% (Fig. 3a). Morphometry of the embryos (whole weight and length) recorded significant decrement at all the doses (10–100 μg/ml) (Fig. 3b). Whole weights of liver, brain and heart showed non-significant decrement at all the said doses (Supplementary Table S4).

ICP-OES analysis of embryos. After 4-days of TiO_2 NPs treatment, the contents of Ti in the chick embryo were measured by ICP-OES. Significantly high levels of Ti was detected (3 times increase) in embryos of eggs treated with 10 μg/ml TiO_2. But, higher dose (100 μg/ml) accounted for a moderate non-significant content of Ti in embryos (Fig. 3c).

Deformity. Control and TiO_2 NPs treated chick embryos were examined as per Hamburger-Hamilton standard that revealed presence of flexed limbs at 10 and 25 μg/ml doses of TiO_2 NPs (Fig. 3d). Also, omphalocele (ventral body wall defect) was observed at 10 μg/ml dose. These deformities were not seen at any of the higher doses (50 and 100 μg/ml). Further confirmation of flexed limbs of 10 and 25 μg/ml TiO_2 NPs treated embryos was obtained by alcian blue- alizarine red staining (Fig. 3e).

Expression of Wnt signaling genes. RT-PCR analysis was performed to assess the effect of TiO_2 NPs on expression of key genes of canonical (CTNNB1, PITX2 and LEF1), non-canonical Wnt/Ca^{2+} (WNT11, PRKCA and CAMK2D) and Planar Cell Polarity (ROCK1 and ROCK2) pathways associated with Wnt signaling. Expression levels of genes of canonical pathway (CTNNB1, PITX2 and LEF1) were downregulated significantly

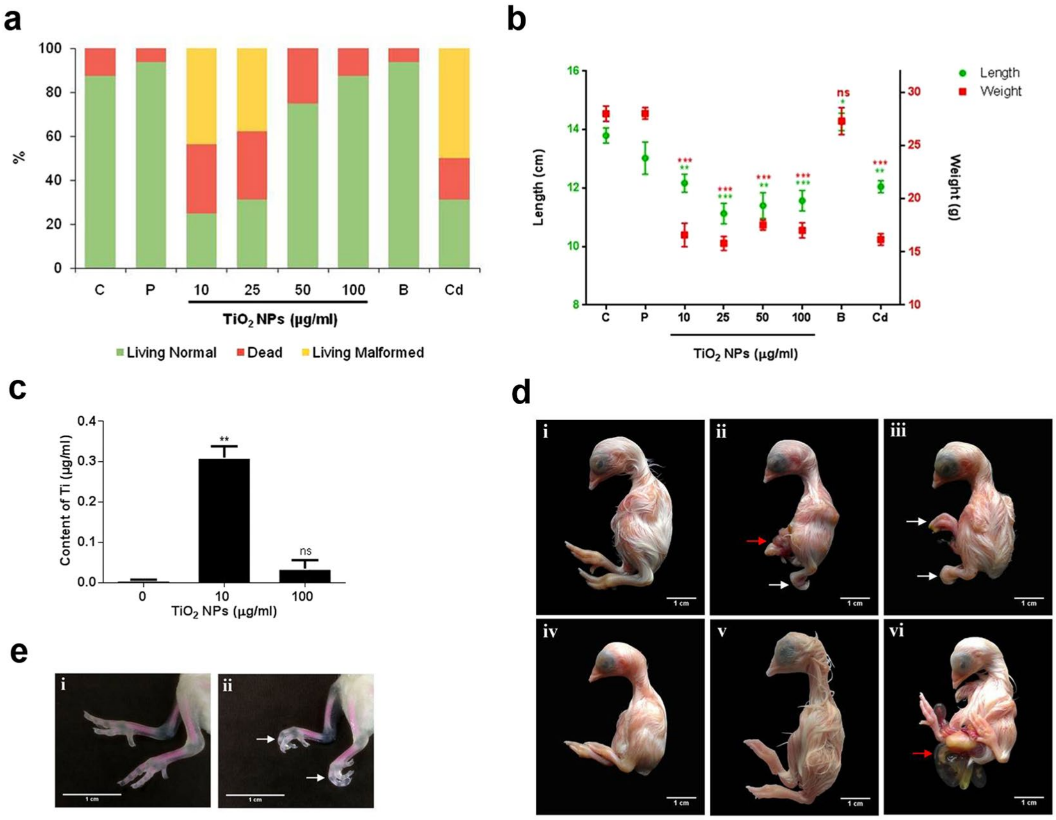

Figure 3. TiO_2 NPs induces developmental deformities in chicken embryo. (**a**) Percentages of living normal, dead and malformed embryos in 19-day-old chick embryos. (**b**) Mean body weight (g) and lengths (cm) of living 19-day-old chick embryos in control and treated groups. (**c**) Concentrations of Ti in embryos of control and TiO_2 NPs-treated group (4 day old) by ICP-OES. (**d**) Chicken-embryo development after 19 days of incubation, control (i), 10–100 µg/ml TiO_2 NPs-treated groups (ii,iii,iv), 10 µg/ml TiO_2 Bulk (v) and 10 µg/ml cadmium chloride (vi), (Scale bar: 1 cm). Embryos treated with 10 µg/ml TiO_2 NPs (ii) exhibits omphalocele (red arrow) & flexed limbs (white arrow). (**e**) Photographs showing endoskeleton (bone and cartilage) of 19-day-old chick embryos, control (i) and TiO_2 NPs–treated (ii) stained with Alizarin red S and alcian blue staining. TiO_2 NPs treated (10 µg/ml) embryos exhibits flexed digits (arrow). The data are expressed as Mean ± SD. Statistical analysis was done by one way ANOVA, $^{*}p \leq 0.05$, $^{**}p < 0.01$, $^{***}p < 0.001$, ns- not significant, C- control, P-placebo, B- TiO_2 Bulk (10 µg/ml), Cd- cadmium chloride (10 µg/ml).

in embryos treated with TiO_2 NPs (10 µg/ml). A Similar trend of significant decrement was also observed in cadmium treated embryos, whereas, TiO_2 bulk treatment could not manifest any significant change (Fig. 4a–c). Expression levels of key genes of non-canonical Wnt/Ca^{2+} Wnt signaling (WNT11, PRKCA and CAMK2D) showed significantly lowered expression levels following TiO_2 NPs or cadmium treatment. However, the TiO_2 bulk treatment showed non-significant changes in the expression levels of the said genes (Fig. 4d–f). mRNA expression of key genes of Planar Cell Polarity pathway (ROCK1 and ROCK2) accounted for non-significant decrement following TiO_2 NPs or cadmium treatment. TiO_2 bulk treatment accounted for moderately significant increment in ROCK1 expression and non-significant increment in expression of ROCK2 (Fig. 4g and h). Expression levels of HOXD13 showed significantly lowered expression levels following TiO_2 NPs or cadmium treatment, whereas, the TiO_2 bulk treatment showed non-significant changes (Fig. 4i).

Somite development. It was observed that 10 µg/ml dose of TiO_2 NPs accounted for 20% decrement in the number of somites after 24 h which was comparable to that of the cadmium treated group, whereas, TiO_2 bulk treatment could not manifest any significant change (Fig. 4j).

Discussion

Nanomaterials have been reported to interact with protein molecules in unique ways and form a 'protein corona' that alters its physicochemical identity and affect its bio-distribution, kinetics and subsequent toxicity[22]. A previous study in our lab had shown that TiO_2 NPs interact with protein components of RPMI-1640 and result in higher indices of intermolecular interaction[23]. Egg albumen is reservoir of protein in an avian egg that meets the nutritional requirements of an embryo. Besides egg shell, shell membrane and chorio-allantoic membrane; egg albumen also regulates the trafficking of exogenous elements by acting as a natural biological barrier[24]. In the present study, a dose dependent increase in density of albumen was observed following addition of TiO_2 NPs. But, relatively lowest density observed at 10 µg/ml hints at effective dispersion of TiO_2 NPs in egg albumen. Higher

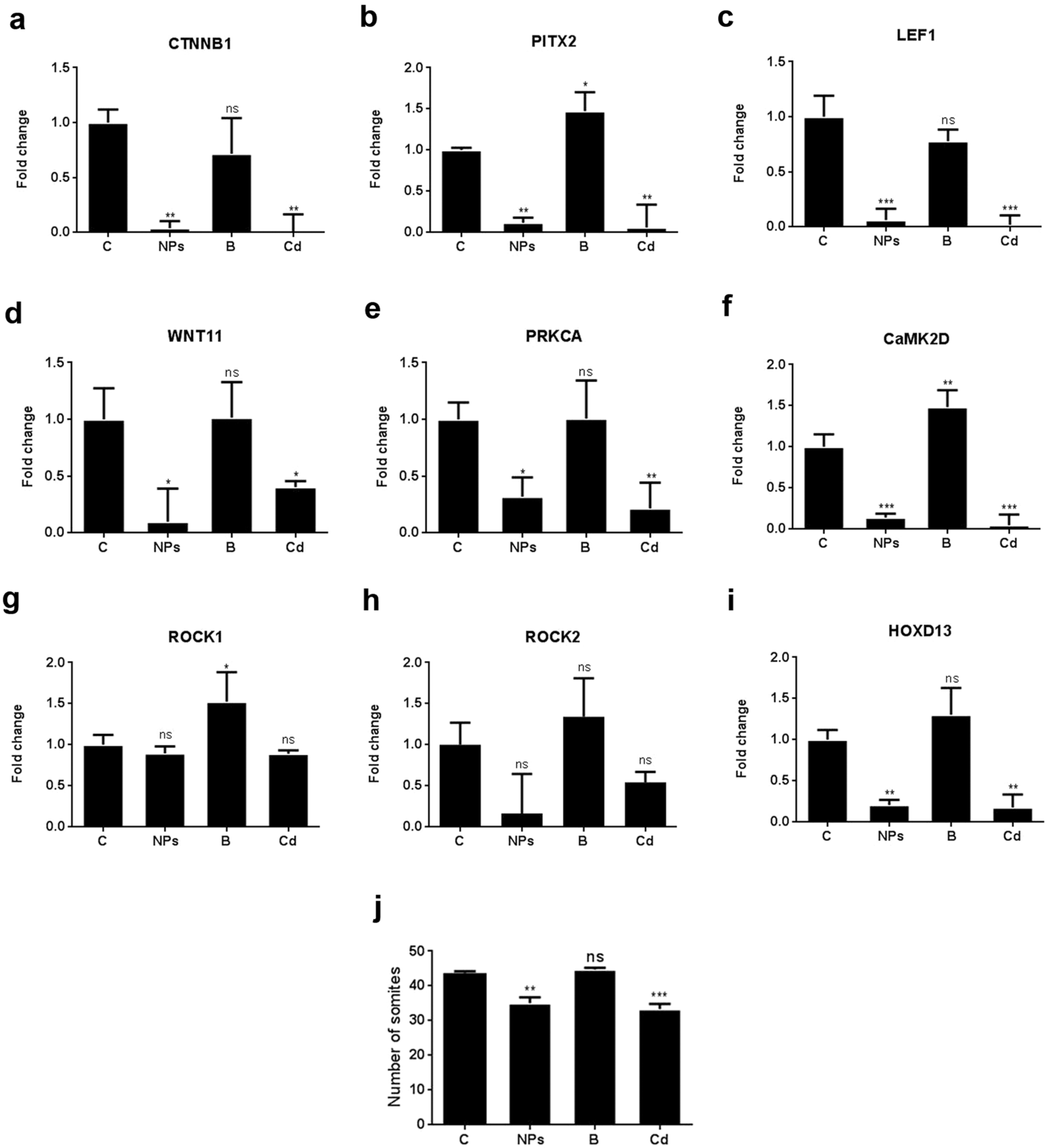

Figure 4. Expression of Wnt signaling pathway-related genes in TiO_2 NPs-treated chicken embryos. The expression of Wnt signaling pathway-related genes (**a**–**h**) including CTNNB1, PITX2, LEF1, WNT11, PRKCA, CAMK2D, ROCK1 and ROCK2 and (**i**) limb development gene HOXD13 was analyzed using reverse transcription polymerase chain reaction (RT-PCR) in control and TiO_2 NPs-treated embryos (n = 3), 4 h after treatment in shell-less culture at 60 h. All the Wnt signaling pathway related genes and limb development gene were downregulated in TiO_2 NPs-treated embryos compared to those of control embryos. *$p < 0.05$, **$p < 0.01$, ***$p < 0.001$, ns = not significant. (**j**) Somite numbers in control and TiO_2 NPs-treated embryos 24 h after treatment in shell-less culture (HH-23). There is a reduction in the number of somites in TiO_2 NPs-treated embryos as compared to the control embryos. The data are expressed as Mean ± SD. Statistical analysis was done by one way ANOVA followed by Dunnett's test. *$p < 0.05$, **$p < 0.01$, ***$p < 0.001$, ns = not significant.

intermolecular forces and cohesion are the key factors that determine viscosity and surface tension of liquids. In our study, a dose dependent decrement in viscosity and a reciprocal increment in surface tension are in support of our claim that higher intermolecular forces are as a result of higher concentration of TiO_2 NPs. Friccohesity is a product of frictional and cohesive forces within similar (protein-protein) and dissimilar (protein-nanoparticle) molecules[25]. A dose dependent decrement in friccohesity suggests weaker inter conversion between cohesive and frictional forces implying towards a stronger nanoparticles-egg albumen interaction. Also, a decrement in activation energy is an indicator of increased proportion of collision/chemical reaction between the test compounds[23]. Relatively higher indices of activation energy recorded in TiO_2 NPs + albumen (10 µg/ml) is suggestive of more quantum of interaction between TiO_2 NPs and egg albumen. Molecular radii play an important role in dispersion of nanometals and its impact on biological systems. A dose dependent increment in molecular radii resulting due to TiO_2 NPs-egg albumen interactions implies towards formation of nanoparticle agglomerates at higher doses.

TiO_2 NPs + albumen recorded a shift in H-O-H stretching peak to 3478 cm^{-1} confirming interaction between TiO_2 NPs and albumen. Further a shift in peak from 2071 cm^{-1} (in albumen) to 2083 cm^{-1} (TiO_2 NPs + albumen) is attributable to interaction between C-O and amide groups of amino acids present in albumen. Peaks observed in the amide I and II secondary fingerprint region (in albumen) at 1651 cm^{-1} and 1642 cm^{-1} are attributable to C=O stretching and H-O-H bending respectively. However, a minor shift in C=O stretching and depletion of H-O-H bending (at 1641 cm^{-1}) was possibly on account of electrostatic interaction due to Vander Waal forces taking place between albumen and TiO_2 NPs. Peak in amide III region (at 1243 cm^{-1}) in albumen occurs due to N-H bending and C-N stretching of amino groups but, TiO_2 NPs + albumen recorded a shift (at 1551 cm^{-1}) from amide III to amide II region. This shift also portrays major conformational changes in secondary components (α helices and β sheet) of proteins possibly due to their interaction with TiO_2 NPs. Fourier-self deconvolution approach was employed to assess secondary conformational changes in amide I and II region. Venyaminov and Kalnin[26] had reported that amide peak at 1610 ± 4 corresponds to NH bending of CO-NH_2 bond in glutamine. In our study, amide peak at 1610 cm^{-1} in TiO_2 NPs + albumen indicates possible deformity of glutamate in egg albumen. Role of glutamate in nutrition and metabolism is well reported[27] and hence impact of structurally altered glutamate on developing chicken embryo is postulated herein. Further, an increase in β sheet and α helices in TiO_2 NPs + albumen are possibly due to TiO_2 NPs mediated conformational changes, formation of aggregates or amyloids with protein moieties in egg albumen. These findings are the first to showcase interaction of TiO_2 NPs with egg albumen and the said physicochemical alterations.

Interaction of TiO_2 NPs with egg albumen prompted us to assess its impact on embryonic development using chicken egg as a model. Significant reduction in morphometric indices (body weight and length) and higher percentage mortality was recorded in developing chicken embryos at lower doses of TiO_2 NPs (10 µg/ml). But, the higher doses of TiO_2 NPs (50 or 100 µg/ml) failed to elicit a dose-dependent toxicological response possibly because TiO_2 NPs underwent physicochemical alterations as evidenced by relatively higher indices of density, viscosity and friccohesity coupled with lower activation energy hinting at formation of NP agglomerates. Whereas, lower extent of NP-egg albumen interactions observed at 10 µg/ml of TiO_2 NPs was instrumental in its effective bio-distribution and manifested said toxicity. Percentage mortality of bulk TiO_2 treated chicken embryos was comparable to that of higher doses (50 or 100 µg/ml) of TiO_2 NPs thus providing conclusive evidence that an altered physicochemical identity of NPs failed to induce a dose dependent toxicity in chicken embryos. Nanoparticles are known to cross biological barriers like the blood brain barrier and blood placenta barrier[28]. The results obtained herein indicate that the TiO_2 NPs could cross biological barriers within an avian egg and reach the embryo. The same was confirmed by ICP-OES studies that revealed presence of higher levels of TiO_2 NPs in the embryonic tissue at the lower dose (10 µg/ml).

Omphalocele is a ventral body wall defect and is accompanied by herniation of midgut into the abdominal cavity, failure in fusion of the anterior abdominal wall with 1/3000 frequency of occurrence in human population[29]. Teratogenic agents such as cadmium[30], specific radiations[31], fungal toxins[32], etc. are known to induce omphalocele in various animal models. However, no known nanomaterials have been reported to induce omphalocele. Wnt signaling pathway has been implicated in various events of embryonic development such as cell differentiation, survival, migration, proliferation, adhesion and somite formation[33]. Canonical Wnts relay their signal via ß-Catenin pathway that control cell fate determination[33]. Whereas, the non-canonical Wnt signaling either through Wnt/Ca^{2+} pathway or planar cell polarity pathway that controls cell adhesion and movement[33]. Results obtained herein were compared with cadmium induced omphalocele chicken embryo model[30]. PITX2, a bicoid-type homeodomain transcription factor, has known to be regulated by ß-Catenin dependent Wnt pathway[34]. In the Wnt/ß-Catenin pathway, the accumulation of ß-Catenin in the nucleus converts DNA-binding factor, lymphoid enhancing factor-1 (LEF1), to a transcriptional activator and is regulated through direct physical interaction with PITX2 and ß-Catenin[35]. In this study, downregulation in expression levels of CTNNB1, PITX2 and LEF1 following TiO_2 NPs treatment (10 µg/ml) could be a key factor in the disruption of somite myogenesis by inhibiting Wnt/ß-Catenin pathway. It has been postulated that cells from somites migrate into the parietal layer of lateral plate mesoderm (LPM) to assist in forming the lateral body folds[36]. PITX2 is known to regulate cell survival[37] and its downregulation may induce abnormal apoptosis in the somite and LPM that could further interfere with the movement of the lateral body wall folds[29]. These results justify the decrement in somite count obtained in our study following TiO_2 NPs treatment (10 µg/ml). WNT11, a member of the noncanonical Wnts, is an important epithelialization factor acting on the dermomyotome whereas, PRKCA and CaMK2D control actin-cytoskeleton organization and cell contractility[33,38]. Previous studies had implicated PRKCA and CaMK2D (activated by WNT11) in the regulation of cell-cell adhesion molecules (CAMs) such as cadherins. The resultant linkages between E-cadherin and actin filaments reinforce the cell-cell junctional connection[39]. In our study, downregulation of WNT11, PRKCA and CaMK2D genes after TiO_2 NPs treatment (10 µg/ml) possibly interfered with actin-cytoskeleton organization, cell movement and cell adhesion, thus disrupting noncanonical Wnt/Ca^{2+} signaling that resulted in omphalocele. Rho kinases (ROCK) are involved in the regulation of various cellular functions (contraction, adhesion, migration, proliferation and apoptosis) including tissue closure during embryonic development. ROCK1 and ROCK2 mediate signaling from Rho to the actin cytoskeleton in the Wnt non-canonical pathway[40]. ROCK1 knockout (KO), ROCK2 KO, and ROCK1/2 double heterozygous mice has been reported to exhibit omphalocele phenotype due to disorganization of actin filament in the epithelial cells of umbilical ring[41]. Downregulation of ROCK genes following TiO_2 NPs treatment possibly disrupted actomyosin assembly, resulting in the failure of ventral body wall closure resulting in omphalocele. Defects in ventral body wall closure and omphalocele has also been reported with accompanying limb deformities in genetically modified experimental models[42]. *Hox* genes are important regulators of limb pattern in vertebrate development, HOXD13 misexpression in the hindlimb results in shortening of the long bones, including the femur, the tibia, the fibula and the tarsometatarsals[43]. In our study, significantly lowered expression of HOXD13 in TiO_2 NPs treated embryos corroborate with the observed omphalocele. Cadmium is known to use Ca^{2+} ion channels and membrane transporters to enter in to the cells of a developing embryo. Further, it disrupts lateral plate mesodermal cells and induces omphalocele[30]. Therefore, cadmium treated chicken embryos were used as a disease control in our study wherein; expression levels of key genes of the Wnt signaling pathways were comparable to TiO_2 NP treated embryos. TiO_2 NPs are also known to cause free radicals induced cellular damage[6]. Free radical induced disruption of lateral plate mesoderm and somite myogenesis culminating in omphalocele in TiO_2 NPs treated chicken embryos is hypothesized in our study.

Besides their widespread industrial use, TiO_2 NPs have gained prominence in biomedical applications due to their long term photostability, superior biocompatibility, catalytic efficiency and a strong oxidizing power[44,45]. Photodynamic therapy for cancer, cell imaging, genetic engineering, drug delivery and biosensors are some of the reported biomedical applications of TiO_2 NPs[44,45]. Also, their use in diagnosis of cardiovascular diseases, diabetes mellitus, cancer and orthopaedic disorders underlines their prominence. But, omphalocele formation only at sub lethal (lower) concentrations reported herein raises concerns of toxicity benchmarks impacting foetal development. Hence, it raises an urge to study interactions of nanoparticles with biomolecules vis-à-vis particle size or surface modifications prior to their use in diagnostics or biomedical applications.

Conclusion

Nanometal oxides witness a wide range of biomolecules in a physiological environment that can alter their behavior and responses. In the present study, TiO_2 NPs were found to interact with egg albumen as evidenced by changes in their proteinic secondary structure. These interactions could possibly allow TiO_2 NPs to traverse the biological barriers (shell membrane and CAM) within chicken egg and affect the growth and development of embryos and cause malformations like omphalocele and flexed limbs. Also, the observed mortality and significant decrement in morphometry (whole weight and length) are attributable to TiO_2 NPs-albumen interactions. Omphalocele formation in TiO_2 NPs treated groups is possibly due to the disruption of somite myogenesis as evidenced by alterations in expression of key genes of Wnt signaling pathway. Hence, use of TiO_2 NPs in diagnostics and therapy warrants a detailed research in embryos by taking into account its particle size, surface modifications and interaction with biomolecules.

Materials and Methods

Availability of Data and Materials. The datasets supporting the conclusions of this article are included within the article.

Nanoparticles. Titanium (IV) oxide nanopowder (TiO_2 NPs, mixture of Anatase and rutile, Cat. no. 634662, particle size <100 nm, 99.5% purity) was procured from Aldrich (St. Louis, MO, USA). TiO_2 NPs (1 mg/ml) were suspended in water and probe sonicated (LMUC-4, Labman scientific instruments Pvt. Ltd., Kolkata, India) for 30 min. After sonication, the particle size distribution was measured using a 90 plus DLS (Dynamic light scattering) unit from Brookhaven (Holtsville, USA).

Physicochemical analysis. The physicochemical properties such as density, viscosity, surface tension, activation energy, friccohesity and molecular radii were assessed in absence or presence of TiO_2 NPs in egg albumen (freshly collected). TiO_2 NPs were suspended in egg albumen at 1, 5, 10, 25, 50 and 100 μg/ml concentrations. Density of TiO_2 NPs in water and egg albumen were determined with Anton Paar Density and Sound velocity Meter (DSA 5000 M). Density was calculated using equation 1:

$$\rho = \rho^\circ + S_\rho m + S'_\rho m^2 \tag{1}$$

(ρ° at $m \rightarrow 0$ is limiting density, $S\rho$ is the 1st slope)

Viscosity was measured as viscous flow times (VFT) using Borosil Mansingh Survismeter[23] at physiological temperature of 37 °C (LAUDA ALPHA RA 8 thermostat) and calculated by equation 2:

$$\eta = \left(\frac{t}{t_\circ}\right)\left(\frac{\rho}{\rho_\circ}\right)\eta_\circ \tag{2}$$

($\eta_\circ$ is viscosity of water and $t_\circ$, t are flow times of solvent and mixtures respectively)

The η data were regressed with following equation 3:

$$\eta = \eta^\circ + S_\eta m \tag{3}$$

(η° atm $\rightarrow 0$ is limiting viscosity; S_η is the 1st degree slope).

Surface tension was measured by counting pendent drop numbers (PDN) using Borosil Mansingh Survismeter and calculated by equation 4:

$$\gamma = \left(\frac{\eta_\circ}{\eta}\right)\left(\frac{\rho_\circ}{\rho}\right)\gamma_\circ \tag{4}$$

($\gamma_\circ$ is surface tension of water, $\eta_\circ$ and η are pendent drop numbers of medium and solutions respectively)
The γ data were regressed for limiting values γ° at m $\rightarrow$ 0 with following equation 5:

$$\gamma = \gamma^\circ + S_\gamma m \tag{5}$$

(γ° is limiting surface tension, and S_γ is the 1st degree slope)
Friccohesity was calculated using Mansingh equation 6[46]:

$$\sigma = \sigma_\circ\left[\left(\frac{t}{t_\circ} \pm \frac{B}{t}\right)\left(\frac{\eta}{\eta_\circ} \pm 0.0012(1 - p)\right)\right] \tag{6}$$

(σ is friccohesity, t and $t_\circ$ are the sample and solution viscous flow times respectively, $\eta_\circ$ and η are the pendant drop numbers of medium and solutions respectively)

Reference friccohesity was calculated by equation 7

$$\sigma_\circ = \eta_\circ/\gamma_\circ \tag{7}$$

where, $\eta_\circ$ and $\gamma_\circ$ are the viscosity and surface tension of references respectively.

For activation energy, the partial molar volume V_2 was calculated with following equation 8:

$$V_2 = \left[\frac{1000(\rho^\circ - \rho)}{m\rho^\circ\rho}\right] + \frac{M}{\rho} \tag{8}$$

(M is molar mass, ρ° is density of water and ρ is density of solution)
The V_1 for water or albumen at 37 °C is calculated with equation 9:

$$V_1 = \frac{M}{\rho} \tag{9}$$

V_1 and V_2 are used for calculating activation energy by using equation 10:

$$\Delta\mu_1{}^* = RT\ln\left(\frac{\eta_\circ V_1}{hN}\right) \tag{10}$$

($\Delta\mu_1{}^*$ is activation energy of water or albumen, R is gas constant, h is Planck constant and N is Avogadro number (6.023×10^{23}). Activation energy ($\Delta\mu_2{}^*$ J/mol) was calculated by using equation 11:

$$\Delta\mu_2{}^* = \Delta\mu_1{}^* - \left[\left(\frac{RT}{V_2}\right)((1000\eta) - (V_1 - V_2))\right] \tag{11}$$

Molecular radii r (nm) is calculated by using equation 12:

$$r = \sqrt[3]{\frac{3\phi}{4\pi Nc}} \tag{12}$$

(ϕ is volume fraction of water or albumen entangled with NPs, N is Avogadro number, c is concentration and π is constant).

Each parameter was measured in triplicates.

Spectroscopic characterization. Protein-nanoparticle interaction was identified by Fourier transform infrared (FTIR) spectra (PerkinElmer spectrum 65 series, PerkinElmer, Inc., MA, USA). Sample was prepared by making pellet of 1.5 to 2 mg of sample mixed with 200 mg KBr (AR, Sigma, USA) in the KBr press machine (model Mp-15) at 5 kg/cm^2 pressure for 2 min. After taking background scan, samples were analyzed at 400–4000 cm^{-1}. FTIR direct-transmittance spectroscopy (KBr) was used to indicate the degree to which oxygen groups were removed and the IR absorption of water from the air was mostly eliminated. Each measurement was repeated in triplicates to minimize the error.

Chicken Embryo model and experimental groups. The experimental protocol (MSU-Z/IAEC/03-2017) was approved by the Institutional Animal Ethical Committee (IAEC) and the Committee for the Purpose of Control and Supervision of Experiments on Animals (827/GO/Re/S/04/CPCSEA). Fertilized eggs (55 ± 2.1 g) of White leghorn (*Gallus gallus domesticus*) were obtained from Shakti hatcheries, Sarsa, Gujarat, stored for 2 days at 12 °C and then incubated under standard conditions (37.5 °C, humidity 60%) for 48 hours and guidelines of Committee for the Purpose of Control and Supervision of Experiments on Animals (CPCSEA) were hereby followed for all the experiments conducted on the chicken embryo. The procedures for *in ovo* experimentation were as per the standard operating protocols of our laboratory. Candling was done to confirm the fertility of eggs and unfertile eggs were discarded. Eggs were randomly divided into six groups of 16 eggs/group viz. control (untreated), placebo (treated with PBS) and TiO_2 treated (10, 25, 50 and 100 µg/ml) groups. TiO_2 NPs powder was suspended in saline (1 mg/ml) and sonicated (LMUC-4, Labman scientific instruments Pvt. Ltd. Kolkata, India) for 30 min. Further, TiO_2 NPs were diluted to 10, 25, 50 and 100 µg/ml doses. Test samples were injected *in ovo* (0.3 ml/egg) in airspace using sterile 1 ml tuberculin syringe and incubated for 18 days.

Gene	Gene Name	Accession number	Primer Sequence (5′-3′)
GAPDH	Glyceraldehyde 3-phosphate dehydrogenase	NM_204305.1	F:-ACTGTCAAGGCTGAGAACGG R:-ACCTGCATCTGCCCATTTGA
HOXD13	Homeobox D-13	NM_205434.1	F:-TCTGGCTAATGGCTGGAACG R:-ATCTCGGGCTGGTTTAGTGC
CTNNB1	ß-catenin	NM_205081.1	F:-GTCCTGTATGAGTGGGAGCA R:-GTTTCGGGGAACATAGCAGAA
PITX2	Paired-like homeodomain 2	NM_205010.1	F:-CGATGAGTTGCATGAAGGAC R:-AGGAGGAAGGTGAGGAGGAG
LEF1	Lymphoid enhancer-binding factor 1	XM_015276137.1	F:-TCACCTACAGCGATGAGCAC R:-TATCAGGAGCTGGAGGATGC
WNT11	Wingless-type MMTV integration site family, member 11	XM_015280851.1	F:-TTCATCTTTGGCCCTGAATC R:-AGCTCGATGGATGAGCAGTT
PRKCA	Protein kinase C	XM_004946229.2	F:-ACAACCAGGACCTTCTGTGG R:-TCTCGTAGAGCAGCACTCCA
CAMK2D	Calcium/calmodulin-dependent protein kinase II delta	XM_015276279.1	F:-GCCAATCCACACCATTATCC R:-CCATCCATGTACTGCGTGAG
ROCK1	Rho-associated, coiled-coil containing protein kinase 1	XM_015277931.1	F:-TGACTGGTGGTCAGTTGGAG R:TAGAGATCTCGTTGTCATCAGG
ROCK2	Rho-associated, coiled-coil containing protein kinase 2	XM_015276085.1	F:-GACTGGTGGTCCGTAGGAGT R:-GCAGTCTCTCGGATGTTGTC

Table 1. Primers used for RT-PCR.

Autopsy, morphometry and staining. On 19th day, the experiment was terminated by opening the eggs and the viable embryos were weighed and decapitated. The morphology of the embryos was examined according to the Hamburger and Hamilton[47] standards and ratios of live vs. dead/malformed were recorded. Deformities of the head, limbs, body and tail were observed under a dissecting microscope and photographed with a digital (Nikon coolpix p900) camera. Two embryos per group were processed for Alizarine-alcian blue staining[48]. Briefly, skin and viscera was removed and embryos were fixed in 96% ethanol for 3 days followed by acetone for 2 days. Later, embryos were then rinsed in ethanol for 1–2 h and stained with Alizarine-alcian blue stain (0.015% Alcian blue, 0.005% Alizarin red in 70% ethanol, 20% acetic acid and 10% dH_2O) at 37 °C for 4 h. Embryos were rinsed in ethanol and running tap water for one hour each and muscles were cleared in an aqueous solution of 1% potassium hydroxide. De-staining of embryos was done in a graded series of glycerol/potassium hydroxide (20% glycerol/0.8% KOH, 50% glycerol/ 0.5% KOH and 80% glycerol/0.2% KOH respectively) and stored in 100% glycerol.

Inductively coupled plasma optical emission spectroscopy (ICP-OES). Four days old control and treated eggs (three per group) were opened and embryos were digested overnight at 40 °C in 6 ml of conc. nitric acid and 3 ml of hydrogen peroxide. Contents were heated in an oven (110 °C) for 2 h, cooled at room temperature and diluted with 11 ml of dH_2O. The concentrations of nanosized particles in the embryo were quantified by ICP-OES[49].

Shell-less culture and dosing. In a separate set of experiment, procured eggs were incubated for 60 h in standard conditions and later were explanted into shell-less culture as per Dugan, *et al.*[50]. The embryos were divided into four groups of six eggs each viz control (50 µl PBS), positive control (50 µl of 50 µM $CdCl_2$), TiO_2 NPs treated (50 µl of 10 µg/ml) and bulk TiO_2 (50 µl of 10 µg/ml). Dosing was done directly on blastodisc using a micropipette and embryos were incubated for 4 h or 24 h.

Autopsy, RNA isolation and qPCR study. Developing embryonal discs (three per group, HH 17; whole embryo) were transferred in RNA later solution (Invitrogen, California, USA). Total RNA was isolated using TRIzol reagent (Invitrogen, California, USA) and cDNA was synthesized by reverse transcription of 1 µg of total RNA using iScript cDNA Synthesis kit (BIORAD, California, USA). For HOXD13, total RNA was isolated from limb bud of 4 day old control and treated embryos. Quantitative RT-PCR was performed using SYBR Select Master Mix (Applied Biosystems) in QuantStudio12K (Life Technologies) real-time PCR machine with primers (Table 1) to detect selected messenger RNA (mRNA) targets. The relative mRNA expression levels were normalized against expression levels of GAPDH for each sample and analyzed using $2^{-\Delta\Delta CT}$ method[51].

Somite development. The embryos (three per group) were dissected from their membranes 24 hours after treatment (HH 23) and inspected using the dissecting microscope to count somite numbers.

Statistical analysis. Data analysis was carried out by unpaired Student's t-test or one way analysis of variance (ANOVA) using Graph Pad Prism 6.0 (CA, USA). Differences between control and treatment groups were deemed to be significant when $P < 0.05$.

References

1. Oberdörster, G., Oberdörster, E. & Oberdörster, J. Nanotoxicology: an emerging discipline evolving from studies of ultrafine particles. *Environmental health perspectives* **113**, 823 (2005).
2. Nel, A., Xia, T., Mädler, L. & Li, N. Toxic potential of materials at the nanolevel. *science* **311**, 622–627 (2006).

3. Vance, M. E. *et al*. Nanotechnology in the real world: Redeveloping the nanomaterial consumer products inventory. *Beilstein journal of nanotechnology* **6**, 1769 (2015).
4. Dalai, S., Pakrashi, S., Chandrasekaran, N. & Mukherjee, A. Acute toxicity of TiO2 nanoparticles to Ceriodaphnia dubia under visible light and dark conditions in a freshwater system. *PLoS One* **8**, e62970 (2013).
5. Maurer-Jones, M. A., Gunsolus, I. L., Murphy, C. J. & Haynes, C. L. Toxicity of engineered nanoparticles in the environment. *Analytical chemistry* **85**, 3036–3049 (2013).
6. Shukla, R. K. *et al*. TiO2 nanoparticles induce oxidative DNA damage and apoptosis in human liver cells. *Nanotoxicology* **7**, 48–60 (2013).
7. Lai, J. C. *et al*. Exposure to titanium dioxide and other metallic oxide nanoparticles induces cytotoxicity on human neural cells and fibroblasts. *International journal of nanomedicine* **3**, 533 (2008).
8. Hussain, S., Hess, K., Gearhart, J., Geiss, K. & Schlager, J. *In vitro* toxicity of nanoparticles in BRL 3A rat liver cells. *Toxicology in vitro* **19**, 975–983 (2005).
9. Li, Y. *et al*. Molecular control of TiO2-NPs toxicity formation at predicted environmental relevant concentrations by Mn-SODs proteins. *PLoS One* **7**, e44688 (2012).
10. Hu, C. *et al*. Toxicological effects of TiO 2 and ZnO nanoparticles in soil on earthworm Eisenia fetida. *Soil Biology and Biochemistry* **42**, 586–591 (2010).
11. Gupta, G. S., Kumar, A., Shanker, R. & Dhawan, A. Assessment of agglomeration, co-sedimentation and trophic transfer of titanium dioxide nanoparticles in a laboratory-scale predator-prey model system. *Scientific reports* **6**, 31422 (2016).
12. Clemente, Z., Castro, V., Moura, M., Jonsson, C. & Fraceto, L. Toxicity assessment of TiO 2 nanoparticles in zebrafish embryos under different exposure conditions. *Aquatic toxicology* **147**, 129–139 (2014).
13. Linhua, H., Zhenyu, W. & Baoshan, X. Effect of sub-acute exposure to TiO2 nanoparticles on oxidative stress and histopathological changes in Juvenile Carp (Cyprinus carpio). *Journal of Environmental Sciences* **21**, 1459–1466 (2009).
14. Zhu, X., Zhou, J. & Cai, Z. TiO2 nanoparticles in the marine environment: Impact on the toxicity of tributyltin to abalone (Haliotis diversicolor supertexta) embryos. *Environmental science & technology* **45**, 3753–3758 (2011).
15. Mohammadipour, A. *et al*. Maternal exposure to titanium dioxide nanoparticles during pregnancy; impaired memory and decreased hippocampal cell proliferation in rat offspring. *Environmental toxicology and pharmacology* **37**, 617–625 (2014).
16. Wierzbicki, M., Sawosz, E. & Grodzik, M. Caveolin-1 localization in chicken embryo chorioallantoic membrane treated with diamond and graphite nanoparticles. *Brzozowski m., głogowski r., grzeszczak-pytlak a. Reproduc-tive efficiency of mink females, selected for weaned litter size after first season of repro-duction* **5**, 133 (2012).
17. Pineda, L., Sawosz, E., Vadalasetty, K. & Chwalibog, A. Effect of copper nanoparticles on metabolic rate and development of chicken embryos. *Animal feed science and technology* **186**, 125–129 (2013).
18. Wierzbicki, M. *et al*. Carbon nanoparticles downregulate expression of basic fibroblast growth factor in the heart during embryogenesis. *International journal of nanomedicine* **8**, 3427 (2013).
19. Prasek, M. *et al*. Influence of nanoparticles of platinum on chicken embryo development and brain morphology. *Nanoscale research letters* **8**, 251 (2013).
20. Szmidt, M. *et al*. Toxicity of different forms of graphene in a chicken embryo model. *Environmental Science and Pollution Research* **23**, 19940–19948 (2016).
21. Hotowy, A. *et al*. Silver nanoparticles administered to chicken affect VEGFA and FGF2 gene expression in breast muscle and heart. *Nanoscale research letters* **7**, 418 (2012).
22. Walkey, C. D. & Chan, W. C. Understanding and controlling the interaction of nanomaterials with proteins in a physiological environment. *Chemical Society Reviews* **41**, 2780–2799 (2012).
23. Patel, S. *et al*. DNA binding and dispersion activities of titanium dioxide nanoparticles with UV/vis spectrophotometry, fluorescence spectroscopy and physicochemical analysis at physiological temperature. *Journal of Molecular Liquids* **213**, 304–311 (2016).
24. Willems, E., Decuypere, E., Buyse, J. & Everaert, N. Importance of albumen during embryonic development in avian species, with emphasis on domestic chicken. *World's poultry science journal* **70**, 503–518 (2014).
25. Singh, M. Study of apparent molal volume and viscosity of mutual citric acid and disodium hydrogen orthophosphate aqueous systems. *Journal of Chemical Sciences* **118**, 269–274 (2006).
26. Venyaminov, S. Y. & Kalnin, N. Quantitative IR spectrophotometry of peptide compounds in water (H2O) solutions. II. Amide absorption bands of polypeptides and fibrous proteins in α-, β-, and random coil conformations. *Biopolymers* **30**, 1259–1271 (1990).
27. Brosnan, J. T. & Brosnan, M. E. Glutamate: a truly functional amino acid. *Amino acids* **45**, 413–418 (2013).
28. Rollerova, E. *et al*. Titanium dioxide nanoparticles: some aspects of toxicity/focus on the development. *Endocrine regulations* **49**, 97–112 (2015).
29. Doi, T., Puri, P., Bannigan, J. & Thompson, J. Altered PITX2 and LEF1 gene expression in the cadmium-induced omphalocele in the chick model. *Pediatric Surgery International* **27**, 495–499 (2011).
30. Thompson, J. M. & Bannigan, J. G. Omphalocele induction in the chick embryo by administration of cadmium. *Journal of pediatric surgery* **42**, 1703–1709 (2007).
31. Pampfer, S. & Streffer, C. Prenatal death and malformations after irradiation of mouse zygotes with neutrons or X-rays. *Teratology* **37**, 599–607 (1988).
32. Wangikar, P., Dwivedi, P. & Sinha, N. Effect in rats of simultaneous prenatal exposure to ochratoxin A and aflatoxin B1. I. Maternal toxicity and fetal malformations. *Birth defects research Part B: Developmental and reproductive toxicology* **71**, 343–351 (2004).
33. Doi, T., Puri, P., Bannigan, J. & Thompson, J. Disruption of noncanonical Wnt/CA 2+ pathway in the cadmium-induced omphalocele in the chick model. *Journal of pediatric surgery* **45**, 1645–1649 (2010).
34. Kioussi, C. *et al*. Identification of a Wnt/Dvl/β-Catenin → Pitx2 pathway mediating cell-type-specific proliferation during development. *Cell* **111**, 673–685 (2002).
35. Vadlamudi, U. *et al*. PITX2, β-catenin and LEF-1 interact to synergistically regulate the LEF-1 promoter. *Journal of cell science* **118**, 1129–1137 (2005).
36. Burke, A. C. & Nowicki, J. A new view of patterning domains in the vertebrate mesoderm. *Developmental cell* **4**, 159–165 (2003).
37. Shih, H. P., Gross, M. K. & Kioussi, C. Cranial muscle defects of Pitx2 mutants result from specification defects in the first branchial arch. *Proceedings of the National Academy of Sciences* **104**, 5907–5912 (2007).
38. Geetha-Loganathan, P., Nimmagadda, S., Huang, R., Christ, B. & Scaal, M. Regulation of ectodermal Wnt6 expression by the neural tube is transduced by dermomyotomal Wnt11: a mechanism of dermomyotomal lip sustainment. *Development* **133**, 2897–2904 (2006).
39. Ozaki, M., Ogita, H. & Takai, Y. Involvement of integrin-induced activation of protein kinase C in the formation of adherens junctions. *Genes to Cells* **12**, 651–662 (2007).
40. Shi, J. & Wei, L. Rho kinase in the regulation of cell death and survival. *Archivum immunologiae et therapiae experimentalis* **55**, 61–75 (2007).
41. Shimizu, Y. *et al*. ROCK-I regulates closure of the eyelids and ventral body wall by inducing assembly of actomyosin bundles. *J Cell Biol* **168**, 941–953 (2005).
42. Matsumaru, D. *et al*. Genetic analysis of Hedgehog signaling in ventral body wall development and the onset of omphalocele formation. *PloS one* **6**, e16260 (2011).

43. Goff, D. J. & Tabin, C. J. Analysis of Hoxd-13 and Hoxd-11 misexpression in chick limb buds reveals that Hox genes affect both bone condensation and growth. *Development* **124**, 627–636 (1997).
44. Wu, S., Weng, Z., Liu, X., Yeung, K. & Chu, P. Functionalized TiO2 based nanomaterials for biomedical applications. *Advanced Functional Materials* **24**, 5464–5481 (2014).
45. Yin, Z. F., Wu, L., Yang, H. G. & Su, Y. H. Recent progress in biomedical applications of titanium dioxide. *Physical Chemistry Chemical Physics* **15**, 4844–4858 (2013).
46. Chandra, A., Patidar, V., Singh, M. & Kale, R. Physicochemical and friccohesity study of glycine, L-alanine and L-phenylalanine with aqueous methyltrioctylammonium and cetylpyridinium chloride from T = (293.15 to 308.15) K. *The Journal of Chemical Thermodynamics* **65**, 18–28 (2013).
47. Hamburger, V. & Hamilton, H. L. A series of normal stages in the development of the chick embryo. *Journal of morphology* **88**, 49–92 (1951).
48. Lamb, K. J. *et al*. Diverse range of fixed positional deformities and bone growth restraint provoked by flaccid paralysis in embryonic chicks. *International journal of experimental pathology* **84**, 191–199 (2003).
49. Bryszewska, M. A., Hannam, S. E., Olivas, R. M. & Camara, C. Direct arsenic determination in exposed embryos of zebrafish (Danio rerio) with Zeeman electrothermal atomic absorption spectrophotometry. *Spectroscopy Letters* **42**, 363–369 (2009).
50. Dugan, J. D., Lawton, M. T., Glaser, B. & Brem, H. A new technique for explantation and *in vitro* cultivation of chicken embryos. *The Anatomical Record* **229**, 125–128 (1991).
51. Livak, K. J. & Schmittgen, T. D. Analysis of relative gene expression data using real-time quantitative PCR and the $2-\Delta\Delta CT$ method. *methods* **25**, 402–408 (2001).

Acknowledgements
The authors are thankful to Science and Engineering Research Board (SERB-DST) for financial support in form of Major Research Project (SR/SO/AS-45/2011; 2012–2015). Co-ordinator, DBTMSUB-ILSPARE (for technical support), Ms. Dhruva Trivedi (photo-editing), Mr. Dilip Patil (Rubamin Limited, Vadodara for ICP-OES), Ms. Kavita Shirsath and Mr Kapil Upadhyay (technical help) are also acknowledged.

Author Contributions
R.D. conceptualized the idea and with S.P. designed the study. S.P. and S.J. conducted experiments on chick embryo toxicity whereas, R.C. performed physicochemical studies and later, M.S., and R.C. did data analysis. R.D., S.P. and M.S. drafted the manuscript with inputs from S.T., S.J. and R.C. All authors gave intellectual input to the study and approved the final version of the manuscript.

Additional Information
Supplementary information accompanies this paper at https://doi.org/10.1038/s41598-018-23215-7.

Competing Interests: The authors declare no competing interests.

Publisher's note: Springer Nature remains neutral with regard to jurisdictional claims in published maps and institutional affiliations.

Drug and Chemical Toxicology

ISSN: 0148-0545 (Print) 1525-6014 (Online) Journal homepage: http://www.tandfonline.com/loi/idct20

Toxicity evaluation of magnetic iron oxide nanoparticles reveals neuronal loss in chicken embryo

Shweta Patel, Sarmita Jana, Rajlakshmi Chetty, Sonal Thakore, Man Singh & Ranjitsinh Devkar

DRUG AND CHEMICAL TOXICOLOGY, 2017
https://doi.org/10.1080/01480545.2017.1413110

Taylor & Francis
Taylor & Francis Group

RESEARCH ARTICLE

Toxicity evaluation of magnetic iron oxide nanoparticles reveals neuronal loss in chicken embryo

Shweta Patel[a], Sarmita Jana[a], Rajlakshmi Chetty[b], Sonal Thakore[c], Man Singh[b] and Ranjitsinh Devkar[a]

[a]Department of Zoology, The M.S. University of Baroda, Vadodara, India; [b]School of Chemical sciences, Central University of Gujarat, Gandhinagar, India; [c]Department of Chemistry, The M.S. University of Baroda, Vadodara, India

ABSTRACT
Magnetic iron oxide nanoparticles (IONs) display the ability to cross blood – brain barrier and are envisioned as diagnostic and therapeutic applications, but there are few studies on their potential embryonic toxicity in higher vertebrates. This study investigates interaction of IONs with egg albumen and its subsequent toxicity on chicken embryo. Physicochemical interactions of IONs with egg albumen revealed alterations in friccohesity and secondary structural changes due to weak Vander Waals forces. Toxicity assessment of IONs (10, 25, 50, 100, and 200 µg/ml doses) on chicken embryo accounted for 100% mortality at 200 µg/ml dose due to Fe^{2+} ions overload. However, lower doses (50 and 100 µg/ml) recorded decrement in whole weights and crown-rump lengths of chicken embryo possibly due to ION–albumen interactions. Histology of brain tissue revealed degeneration of neurons (50–60%) at 10–100 µg/ml dose range of IONs. Toxicity studies of IONs with diverse animal models are needed to set a toxicity benchmark for preventing embryonic toxicity prior to its use in biomedical applications. This is the first study on toxicity assessment of IONs in chicken embryo.

ARTICLE HISTORY
Received 14 October 2017
Revised 9 November 2017
Accepted 22 November 2017

KEYWORDS
Iron oxide nanoparticles; chicken embryo; neurotoxicity; teratogeny

Introduction

Commercial use of nanometal oxides in biomedical applications is stemmed due to their bioavailability, enhanced absorption, and their ability to cross biological barriers (Das *et al.* 2009, Wang *et al.* 2010). Although numerous studies focused on investigating their biomedical applications have highlighted versatile nature of nanometal oxides, their toxicity continues to be a major concern (Curwin and Bertke 2011, Brenner *et al.* 2015). Hence, new investigations focused at setting benchmarks for toxicity of nanometal oxides are of pivotal interest and cannot be ignored. Magnetic nanoparticles are reported for their penetrability into human tissues and applications in magnetic resonance imaging (Pankhurst *et al.* 2003, Jae-Hyun *et al.* 2007). Iron oxide nanoparticles (IONs) have been elaborately studied for their targeted drug delivery. Superparamagnetic IONs such as maghemite (γ-Fe_2O_3) and magnetite (Fe_3O_4) are known to generate reactive oxygen species (ROS)-mediated toxicity and peroxidation of membrane lipids (Stohs and Bagchi 1995, Singh *et al.* 2012).

Toxicity of nanomaterials have been extensively reported in *in vitro* models (Sadiq *et al.* 2015, Dönmez Güngüneş *et al.* 2017). Contradicting research reports on toxicity of IONs include, low grade toxicity with intracellular ROS generation (Hussain *et al.* 2005, Jeng and Swanson 2006, Karlsson *et al.* 2009) or the absence of any form of toxicity at lower doses (Karlsson *et al.* 2008). However, higher doses of IONs causes a decline in cellular physiological functions primarily due to oxidative DNA damage (Singh *et al.* 2009), mitochondrial damage, gene transcription modulation, and altered calcium-dependent signaling cascade (Stroh *et al.* 2004). Toxic effects of IONs on developing animal models had reported delayed hatching, embryonic malformations, and mortality in zebrafish embryos (Zhu *et al.* 2012) and, impaired development and delayed maturation in mice (Noori *et al.* 2011) and rabbits (Bourrinet *et al.* 2006).

Chick embryo is a popularly used model to assess developmental toxicity because of an ease in performing *in ovo* manipulations, ready availability, observable developmental stages, and established toxicity endpoints (Coleman 2008, Rashidi and Sottile 2009, Abdolmaleki and Zahri 2016). Toxicity of silver, copper, palladium, and cadmium nanoparticles have been reported on chick embryo (Sawosz *et al.* 2009, Studnicka *et al.* 2009, Prasek *et al.* 2013) but interactions of these nanoparticles with egg albumen have not been taken into account (Celá *et al.* 2014). Due to the prominence of IONs in biomedical applications a detailed scrutiny of its toxicological implications is indispensable. Toxicity of IONs on chick embryo has not yet been studied; hence this inventory is an effort to understand the interaction of IONs with egg albumen and its possible toxic manifestations.

Materials and methods

Nanoparticle and its characterization

Iron (III) oxide nanopowder was procured from Aldrich (St. Louis, MO, USA; Cat. no. 544884, particle size <50 nm). The

CONTACT Ranjitsinh Devkar rv.devkar-zoo@msubaroda.ac.in Department of Zoology, Faculty of Science, The M.S. University of Baroda, Vadodara, India
Supplemental data for this article can be accessed here.

Table 1. Standard specifications about IONs mentioned by Aldrich.

Chemical formula	Color	APS[a] (nm)	TD[b] (g/cc)	Purity (%)
Fe_2O_3	Dark red-brown	35	5.15	99.5

[a]Average particle size measured by Brunauer, Emmett, and Teler (BET) technique.
[b]True density.

characteristics of IONs are mentioned in Table 1. ION (1 mg/ml) was suspended in water and probe sonicated (LMUC-4, Labman scientific instruments Pvt. Ltd., Kolkata, India) for 30 min. Later, the particle size distribution was measured using a 90 plus DLS (Dynamic light scattering) unit (Brookhaven, GA; Holtsville, NY).

Physicochemical analysis

The physicochemical property, friccohesity was assessed in the absence or in the presence of IONs in water, normal saline (0.72% sodium chloride) and egg albumen (freshly collected). IONs were suspended in the above mentioned media at 10, 25, 50, 100, 200, and 500 μg/ml concentrations.

Viscosity was measured as viscous flow times (VFT) using Borosil Mansingh Survismeter (Patel *et al.* 2016) at a physiological temperature of 37 °C (LAUDA ALPHA RA 8 thermostat) and calculated by the following equation:

$$\eta = \left(\frac{t}{t_0}\right)\left(\frac{\rho}{\rho_0}\right)\eta_0$$

(η_0 is viscosity of water and t_0, t are flow times of solvent and mixtures, respectively)

The η data were regressed with the following equation:

$$\eta=\eta^0+S_\eta m$$

(η^0 atm→0 is limiting viscosity; S_η is the first-degree slope).

Surface tension was measured by counting pendent drop numbers (PDN) using Borosil Mansingh Survismeter and calculated by the following equation:

$$\gamma = \left(\frac{\eta_0}{\eta}\right)\left(\frac{\rho_0}{\rho}\right)\gamma_0$$

(γ_0 is surface tension of water, η_0 and η are PDN of medium and solutions respectively)

The γ data were regressed for limiting values γ^0 at m → 0 with the following equation:

$$\gamma=\gamma^0+S_{\gamma}m$$

(γ^0 is limiting surface tension, and $S\gamma$ is the first-degree slope)

Friccohesity was calculated using Mansingh equation (Chandra *et al.* 2013):

$$\sigma = \sigma_o\left[\left(\frac{t}{t_o}\pm\frac{B}{t}\right)\left(\frac{\eta}{\eta_o}\pm 0.0012(1-p)\right)\right]$$

(σ is friccohesity, t and t_0 are the sample and solution viscous flow times respectively, η_0 and η are the pendant drop numbers of medium and solutions, respectively).

Reference friccohesity was calculated by $\sigma_0=\eta_0/\gamma_0$ where, η_0 and γ_0 are the viscosity and surface tension of references, respectively.

Spectroscopic characterization

Protein-nanoparticle interaction was assessed by Fourier transform infrared (FTIR) spectra (Perkin Elmer spectrum 65 series, Perkin Elmer, Inc., Waltham, MA). Sample was prepared by making pellet of 1.5 to 2 mg of sample mixed with 200 mg KBr (AR, Sigma, St. Louis, MO, USA) in the KBr press machine (model Mp-15) at 5 kg/cm^2 pressure for 2 min. After taking background scan, samples were analyzed at 400–4000 cm^{-1}. FTIR direct-transmittance spectroscopy (KBr) was used to indicate the degree to which oxygen groups were removed and the IR absorption of water from the air was mostly eliminated. Each measurement was repeated in triplicates to minimize the error.

Chicken embryo model

The experimental protocol (MSU-Z/IAEC/03-2017) was approved by the Institutional Animal Ethical Committee (IAEC) and the Committee for the Purpose of Control and Supervision of Experiments on Animals (827/GO/Re/S/04/CPCSEA)

Fertilized eggs of White leghorn (*Gallus gallus domesticus*) were obtained from Shakti hatcheries, Sarsa, Gujarat, India. Fertilized eggs (55 ± 2.1 g) were stored for 2 days at 12 °C and then incubated (Bright technologies Inc., Ahmedabad, India) under standard conditions for 48 h in IAEC approved animal house and guidelines of Committee for the Purpose of Control and Supervision of Experiments on Animals (CPCSEA) were hereby followed. Candling was done to confirm the fertility of eggs and unfertile eggs were discarded. Fertilized eggs were randomly divided into 7 groups of 16 eggs/group, namely control (untreated), placebo (treated with saline), and treated with IONs (10, 25, 50, 100, and 200 μg/ml doses). IONs powder was subjected to UV radiation for 20 min, suspended in saline (1 mg/ml) and sonicated (LMUC-4, Labman scientific instruments Pvt. Ltd. Kolkata, India) for 30 min. Fertilized eggs (12 HH stage) of white leghorn were injected (inside a laminar air flow) with IONs (10, 25, 50, 100, and 200 μg/ml). Test samples were injected *in ovo* (0.3 ml/egg in airspace) using sterile 1 ml tuberculin syringe and incubated under standard conditions. At the end of 17 days of incubation (19 day old embryo; HH stage 45), embryos were assessed for mortality and possible developmental deformity.

Morphometry and autopsy of embryos

Shell of control and treated eggs were cut at the broad end by sterile scissors and inner shell membrane was removed to expose the embryo. Viable embryos were removed and made free of placental tissue and fluids prior to weighing (MS-600, American weigh scales Inc., Cumming, GA). Later, the embryos were examined according to the Hamburger and Hamilton (1951) standards and possible malformations (of the head, limbs, body, and tail) were observed under a dissecting microscope. Ratio of live vs. dead/malformed embryos was also recorded. Crown-rump lengths for each embryo were recorded and all embryos were photographed with a digital (Nikon coolpix p900) camera. Later, embryos were decapitated and organs (brain, heart, liver, and spleen) were dissected, weighed, and processed for histopathology.

Microscopic evaluation

Tissue samples of brain, heart, liver, and spleen from control and IONs-treated groups were fixed in 10% buffered formalin (pH 7.2). Later, samples were dehydrated in a graded series of ethanol and embedded in paraffin blocks. Tissue sections (5–6 µm thick) were stained with hematoxylin–eosin (HXE), observed and photographed (Leica DM 2000) at 100× and 400×. Each slide was scored for healthy and degenerating neurons. Multiple random areas in each tissue section were scored on a six-point scale: 0 = no dead neurons, 5 = >0–10%, 30 = >10–50%, 70 = >50–90%, 95 = 90–<100%, and 100 = 100% dead neurons and mean scores were calculated (George *et al.* 2004).

Statistical analysis

Data analysis was carried out by one-way analysis of variance (ANOVA) using Graph Pad Prism 6.0 (La Jolla, CA). Differences with $p < 0.05$ were considered to be statistically significant.

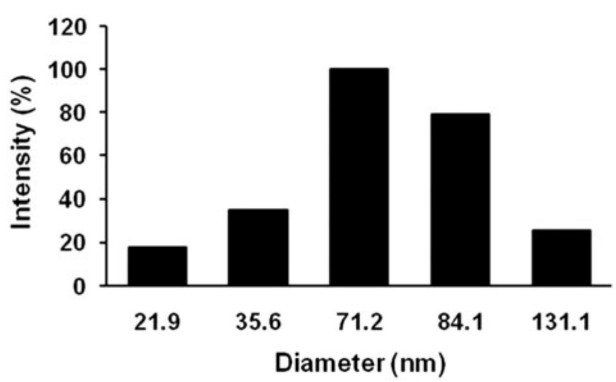

Figure 1. Characterization of IONs using dynamic light scattering.

Results

Characterization of IONs

In DLS analysis, IONs presented a single distribution with peak centered at 71.2 nm. The plot showed that the nanoparticles have a narrow size distribution with an average diameter of about 71.2 nm (Figure 1).

Physicochemical analysis

Changes in egg albumen following its interaction with IONs were studied by assessing its friccohesity, which was calculated taking into account surface tension and viscosity of water, saline or albumen (Table 2). The limiting friccohesity was found to be higher in saline (0.010433 s.m.$^{-1}$) as compared to IONs + albumen (0.001732 s.m.$^{-1}$, Table S1). Saline witnessed 0.04% increase at 200 µg/ml followed by a 0.08% decrement at 500 µg/ml, whereas albumen recorded a steady decrement of 0.01% upto 200 µg/ml (Table S2, Figure 2).

Spectroscopic characterization

Secondary structural changes in native egg albumen were studied in the absence or in the presence of IONs using FTIR spectra (400–4000 cm^{-1}, Figure 3) at 100 µg/ml. Peaks at 3591 and 3534 cm^{-1} obtained in native albumen corresponded to H–O–H asymmetric and symmetric stretching, whereas a peak at 2083 cm^{-1} corresponded to linear C–O group present in amino acids. Peaks at 1643 and 1651 cm^{-1}

Table 2. Viscosity ($\eta \pm 10^{-5}$mPa·s) and surface tension ($\gamma \pm 10^{-2}$mN m^{-1}) of water, saline, and albumen at 37 °C.

Pure solvents	*H*	ϒ
Water	0.696	70
Saline	0.7280945	78.183
Albumen	2.5583631	66.176

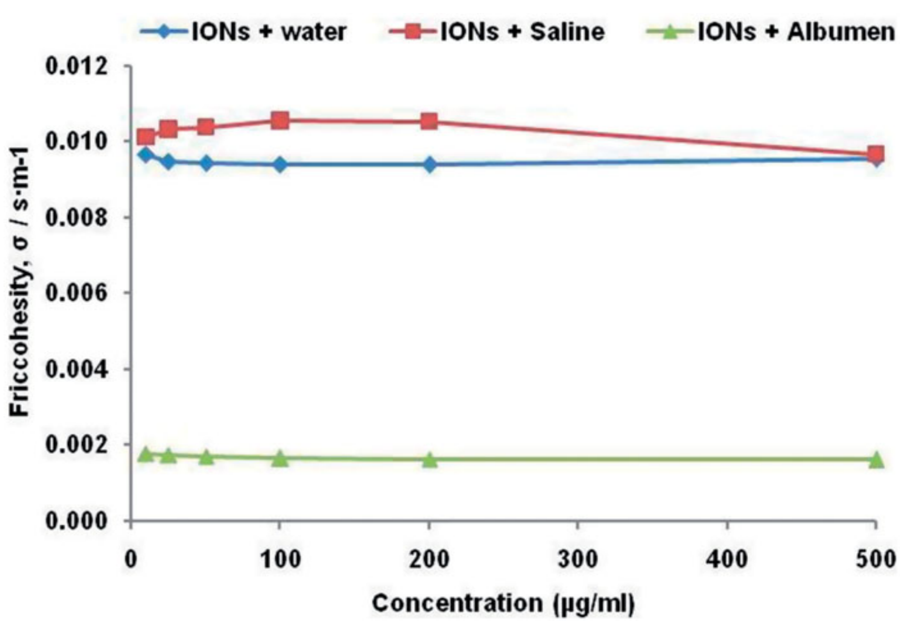

Figure 2. Friccohesity of IONs in water, saline, and albumen.

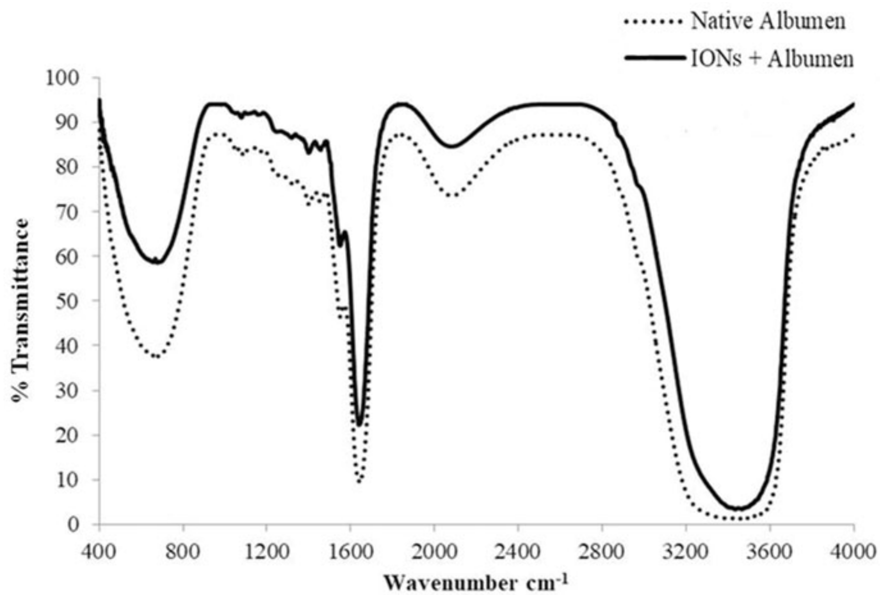

Figure 3. Comparative FTIR spectra of native egg albumen and IONs + Albumen.

Table 3. Percentage of secondary structure components in native egg albumen and IONs + egg albumen at 100 μg/ml.

	% Secondary structure					
	Side chain	β sheet	Random coil	α helix	β turn	β sheet
Native albumen	20.93	39.11	3.30	13.94	11.95	10.76
IONs + albumen	15.41	23.06	9.47	26.56	12.26	13.23

corresponded to amide I region of albumen due to C = O stretching whereas, a peak at 1549 cm^{-1} implies at amide II region due to N–H bend in plane and C–N stretch. Peak at 1453 cm^{-1} is due to CH_2 scissoring vibration and around 1401 cm^{-1} corresponded to C = O stretch of COO^- group. Also, 674 cm^{-1} is mainly due to O = C–N deformation summing up the amide IV region in native albumen. In IONs + albumen there was no distinguishable shift recorded in addition to the peak at 418 cm^{-1} which corresponds to the Fe–O metal oxygen vibrational mode of IONs. An approximation based deconvolution method was used to investigate the secondary structural changes taking place in the amide I region from 1600–1700 cm^{-1}. Figures Supplementary 1 (A, B) shows the secondary derivative Gaussian fitted spectra of the amide I region and the percentage of secondary structural component (Table 3).

Morphometry and autopsy of embryos

IONs-treated eggs recorded ~50% mortality at 10–100 μg/ml doses, but 200 μg/ml accounted for 100% mortality (Figure 4). Body weight and crown-rump length of viable embryos revealed significant decrement at 50 and 100 μg/ml doses (Figure 5(A,B)). No deformities were observed in the Hamburger and Hamilton scoring of viable embryos; hence the same have not been showcased herein.

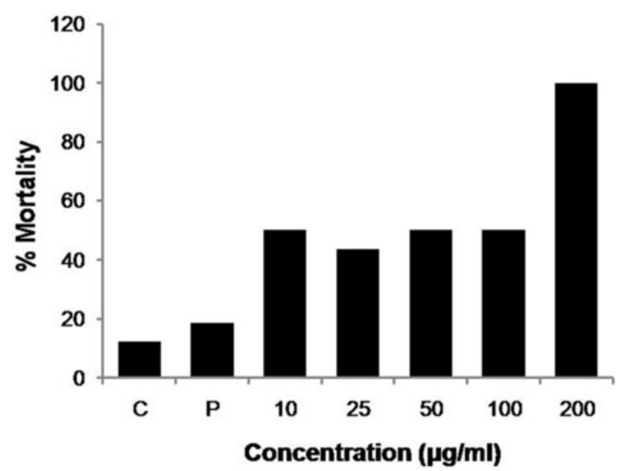

Figure 4. Percentage mortality in control and IONs-treated chick embryos ($N = 16$). C: Control; P: placebo.

Microscopic evaluation

Gravimetry of the liver, brain, heart, and spleen revealed nonsignificant decrements in their weights at all doses of IONs (Table 4). The tissue sections of the liver, heart, and spleen of IONs-treated groups were comparable to that of control; hence the data are not showcased herein. However, the brain sections revealed neuronal loss (scattered dark, shrunken cell with picnotic or small, densely stained nuclei, and eosinophilic cytoplasm) that was significantly higher in 10, 25, 50, and 100 μg/ml treated groups as compared to the control (Figure 6(A)). The tissue sections were scored for degenerating neurons (Figure 6(B)) wherein the results indicated higher percentage of neuronal loss at 10 (50%), 25 (60%), 50 (56.66%), and 100 μg/ml (60%) doses of IONs.

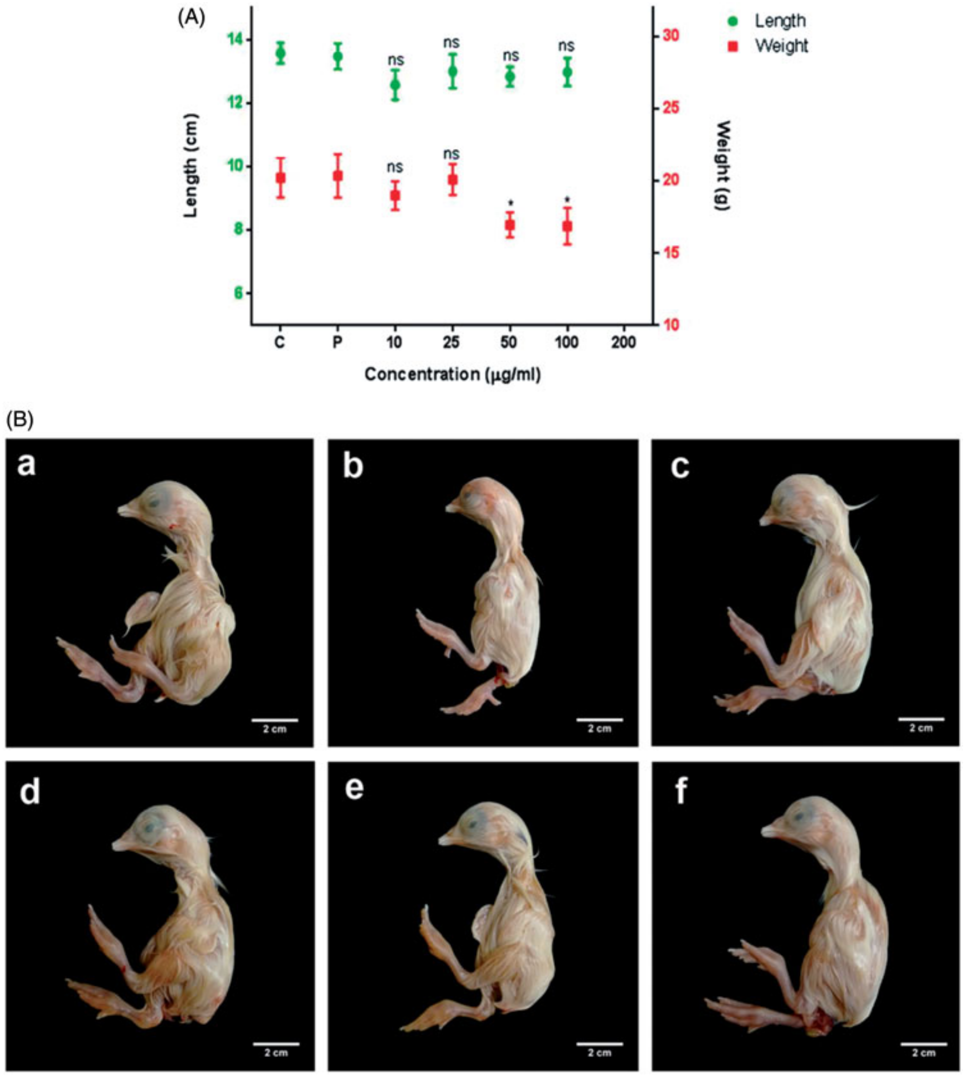

Figure 5. (A) Mean body weight (g) and lengths (cm) of living 19-day-old chick embryos in control and IONs-treated groups. The data are expressed as Mean ± SD. Statistical analysis was done by one-way ANOVA, $*p < 0.05$, ns: nonsignificant; C: control; P: placebo. (B) Chicken-embryo development after 19 days of incubation, a – control, b – placebo and 10–100 µg/ml IONs treated groups (c–f) (Scale bar: 2 cm).

Table 4. Organ weights of chicken embryos treated with IONs.

Organs	Control	Placebo	10 µg/ml	25 µg/ml	50 µg/ml	100 µg/ml	*p* value
Number of embryos	14	13	8	9	8	8	–
Liver, g	0.50 ± 0.04	0.49 ± 0.07	0.34 ± 0.09	0.42 ± 0.03	0.43 ± 0.09	0.42 ± 0.07	Ns
Brain, g	0.45 ± 0.10	0.41 ± 0.04	0.39 ± 0.10	0.35 ± 0.03	0.38 ± 0.08	0.30 ± 0.08	Ns
Heart, g	0.17 ± 0.03	0.16 ± 0.01	0.14 ± 0.02	0.16 ± 0.02	0.16 ± 0.02	0.14 ± 0.01	Ns
Spleen, g	0.02 ± 0.01	0.02 ± 0.00	0.01 ± 0.00	0.02 ± 0.01	0.02 ± 0.00	0.02 ± 0.00	Ns

Discussion

Based on their size, shape, and surface chemistry nanomaterials interact with protein in unique ways such as forming a 'protein corona' (Lynch and Dawson 2008) and undergo changes in their 'biological identity' (Walkey and Chan 2012). They also attain certain levels of Boltzmann distribution energy, enhanced activity and perform localized movements, resulting in alteration in their size, aggregation indices, and interfacial properties. Therefore, interactions of nanomaterials are extensively studied to obtain clarity on their behavior in physiological environment. Friccohesity is a product of frictional and cohesive forces within similar and dissimilar molecules (Patel *et al.* 2016). Fundamentally, higher friccohesity initiates and improves coordination among the molecules in a liquid mixture. A decrement in friccohesity of IONs + albumen observed in our study indicates a poor frictional force and weak molecular interactions. Minor changes observed in IONs + albumen are as a result of weak Vander Waals forces or electrostatic interaction that also provide evidence on binding of iron oxide with albumen.

Nanomaterials interact with protein in unique ways and undergo changes in their size, shape, and surface chemistry (Walkey and Chan 2012) and the same was observed herein, with albumen and IONs. The results obtained in FTIR analysis

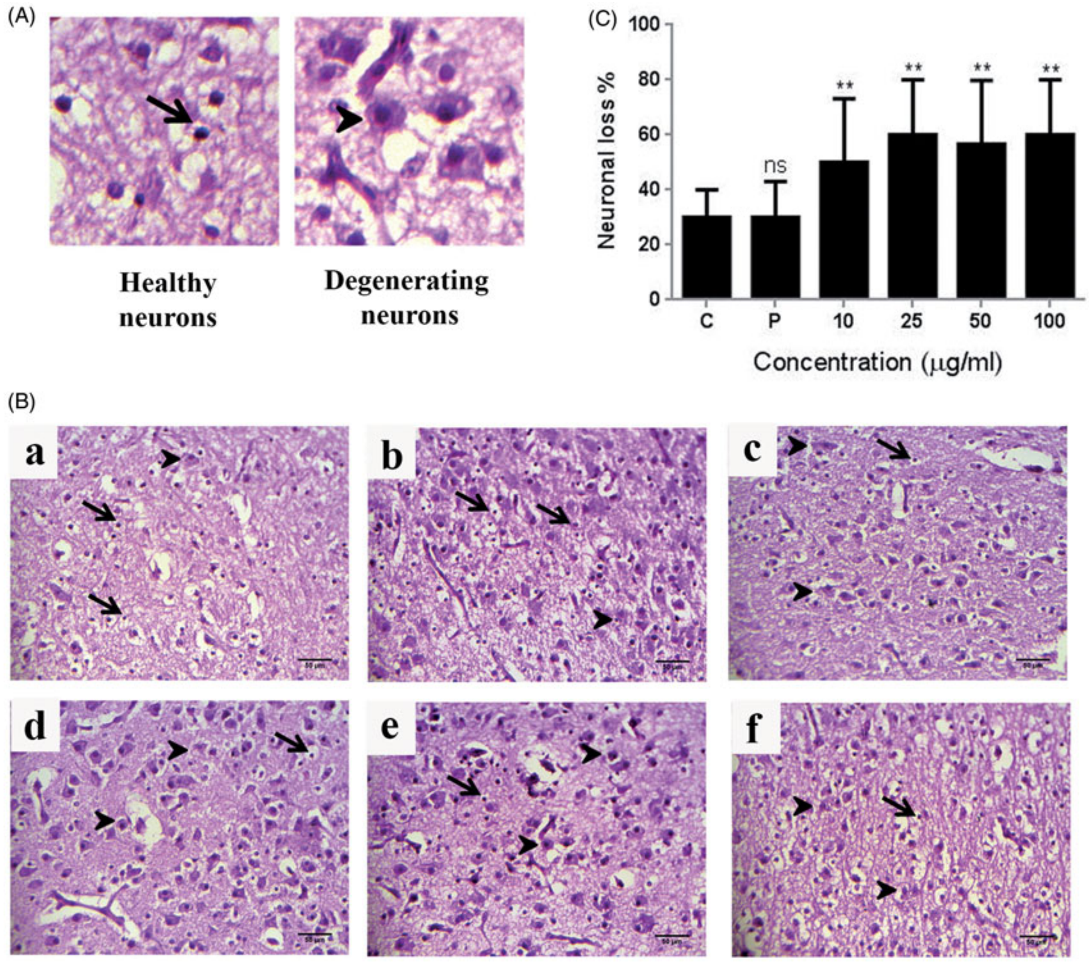

Figure 6. (A) Digitally enlarged images of healthy neuron (arrow) and degenerating neuron (arrowhead) (600×). (B) Histopathological evaluation of brain sections (5 μm) stained with HXE (400×). Degenerating neurons are scattered dark and shrunken cells with picnotic nuclei and eosinophilic cytoplasm. a – control, b – placebo and 10–100 μg/ml IONs-treated groups (c–f) (Scale bar: 50 μm). (C) Percentage neuronal loss in the brain. The data are expressed as Mean ± SD. Statistical analysis was done by one-way ANOVA, $^{**}p \leq 0.01$, ns: nonsignificant; C: control; P: placebo.

of IONs + albumen imply toward loss of molecular activity culminating in subtle changes in their functional moieties. The percentage relative areas of α helices for native egg albumen and IONs + albumen were recorded at 1664 and 1660 cm^{-1}, respectively and were found to be 13.94% and 26.56%. Also, the percentage for β sheet of egg albumen and IONs + albumen were recorded at 1621–1622 cm^{-1} and 1695 cm^{-1}, respectively, and were found to be 49.87% and 36.29%. An increment in α helices and a decrement in β sheet after interaction of albumen with IONs was revealed as per their percentage relative areas. The loops or β turn calculated for relative area at 1681 cm^{-1} increased after interaction of albumen (12.26%) as compared to native albumen (11.95%). The bands at 1647 and 1639 cm^{-1} were assigned for random coil and was found to be 3.30% and 9.47%, respectively, before and after interaction. Hence, it is hypothesized that IONs reach the developing embryo because of its interactions with egg albumen.

Nanomaterials have been reported to be readily adsorbed by various types of proteins that facilitates a strong interaction as seen with cells in culture (Ehrenberg *et al.* 2009) and organ systems (Chonn *et al.* 1992). Subsequently, they are also known to cross biological barriers and functionally modulate physiological environment that often culminates in toxicity (Walkey and Chan 2012). Also, binding capacity of plasma proteins with nanomaterials positively correlates with cellular toxicity (Clift *et al.* 2010). In our study, 10–100 μg/ml dose range of IONs was able to induce ∼50% mortality of chick embryos. It is speculated that the negative impact of IONs on the embryonic development is attributable to the alterations in molecular structure of albumen and subsequent changes in nutritional physiology of developing embryo. Morphometry of viable embryos revealed significant decrement in body weight and crown-rump length at 50 and 100 μg/ml doses. These results are in agreement with the observed decrement in snout vent length in *X. laevis* embryos following IONs treatment (Nations *et al.* 2011). Silver, copper, and palladium nanoparticles have been reported to increase metabolic rates of embryos without inducing deformity (Sawosz *et al.* 2009, Studnicka *et al.* 2009). Since, no skeletal deformity was observed in 10–100 μg/ml dose range of IONs and hence the same is in partial agreement with reports on other nanometals. But, 100% mortality recorded at the highest dose of IONs (200 μg/ml or 3.32 μg IONs/gm of egg) is attributable to Fe^{2+} ions overload coupled with complex interactions of IONs with albumen and other biomolecules.

Bare and surface modified IONs have been reported to cross blood–brain barrier (Wang *et al.* 2010) and induce ROS production in vertebrate embryos. High content of easily peroxidizable unsaturated fatty acids, high oxygen consumption rate, and a primordial antioxidant system in embryonic brain makes it highly vulnerable to ROS-induced damage (Skaper *et al.* 1999). In our study, the weights of key organs (liver, heart, and spleen) of embryos treated with IONs showed nonsignificant decrements and alterations in their histo-architecture. Significantly higher number of degenerating neurons and subsequent neuronal loss were observed following IONs treatment. But, nonsignificant alterations in whole weight of brain of IONs-treated embryos can be a possible case of replacement of neurons by glial cells that needs further scrutiny. Nanometals, such as platinum, have been shown to induce apoptosis in the brain tissue of chick embryo without affecting growth and development (Prasek *et al.* 2013). Low dose of IONs (0.8 mg/kg) has been reported to induce toxicity of liver, kidney and lungs without affecting the brain (Hanini *et al.* 2011). Higher dose range of IONs (30–1000 mg/kg body weight) has been reported to cause weight loss and ATPases inhibition in the brain of rats (Kumari *et al.* 2012, Kumari *et al.* 2013). Also, 50 mg/kg IONs treatment was reported to cross placental barrier and induce testicular toxicity in rat fetuses (Noori *et al.* 2011). These reports provide comprehensive evidence not only on the ability of IONs to cross biological barriers but also to induce systemic toxicity at the said doses. Albumen present in an avian egg also acts as a biological barrier with which IONs is able to interact. This accounts for a decrement in weights of embryos and induce dose-dependent (0.16 to 1.66 μg IONs/g of egg) neuronal loss observed in our study. In humans, iron ions accumulate in brain due to misregulation of iron homeostasis resulting in loss of dopaminergic neurons associated with Parkinson's disease (Ke and Qian 2003), but their possible toxicity on developing fetus and neuronal damage lacks clarity in scientific information. Moreover, the variants of IONs in the form of particle size and surface modifications exhibit toxicities at different doses and hence it is imperative to conduct detailed studies in diverse experimental models.

Conclusions

Nanometal oxides witness a wide range of biomolecules in a physiological environment that can alter their behavior and responses. In our study, IONs were found to interact with egg albumen as evidenced by changes in their proteinic secondary structure. These interactions could possibly allow IONs to traverse the biological barriers within chicken egg and to reach the brain. Also, the observed mortality and neuronal loss are attributable to ION–albumen interactions and production of Fe^{2+} ions by IONs. Hence, the use of IONs in diagnostics and therapy warrants a detailed research on its neurotoxicity in embryos by taking into account its particle size, surface modifications, and interaction with biomolecules.

Acknowledgements

We are thankful to Dr Kishore Rajput for providing help with microscopy and Dr Prakash Pillai and Mr Jaldeep Langhnoja for interpreting the histology results. Ms. Dhruva Trivedi and Ms. Kavita Shirsath are also acknowledged for help rendered.

Disclosure statement

The authors declare that they have no competing interests.

Funding

The authors are thankful to Science and Engineering Research Board (SERB-DST) for financial support in the form of Major Research Project (SR/SO/AS-45/2011; 2012-2015) to RD.

References

Abdolmaleki, A. and Zahri, S., 2016. Comparison of toxicity and teratogenic effects of salen and vo-salen on chicken embryo. *Drug and Chemical Toxicology*, 39 (3), 344–349.

Bourrinet, P., *et al.*, 2006. Preclinical safety and pharmacokinetic profile of ferumoxtran-10, an ultrasmall superparamagnetic iron oxide magnetic resonance contrast agent. *Investigative Radiology*, 41 (3), 313–324.

Brenner, S.A., *et al.*, 2015. Occupational exposure to airborne nanomaterials: an assessment of worker exposure to aerosolized metal oxide nanoparticles in semiconductor wastewater treatment. *Journal of Occupational and Environmental Hygiene*, 12 (7), 469–481.

Celá, P., *et al.*, 2014. Embryonic toxicity of nanoparticles. *Cells, Tissues, Organs*, 199 (1), 1–23.

Chandra, A., *et al.*, 2013. Physicochemical and friccohesity study of glycine, L-alanine and L-phenylalanine with aqueous methyltrioctylammonium and cetylpyridinium chloride from T = (293.15 to 308.15) K. *The Journal of Chemical Thermodynamics*, 65, 18–28.

Chonn, A., Semple, S., and Cullis, P., 1992. Association of blood proteins with large unilamellar liposomes in vivo. Relation to circulation lifetimes. *The Journal of Biological Chemistry*, 267 (26), 18759–18765.

Clift, M.J., *et al.*, 2010. The effects of serum on the toxicity of manufactured nanoparticles. *Toxicology Letters*, 198 (3), 358–365.

Coleman, C.M., 2008. Chicken embryo as a model for regenerative medicine. *Birth Defects Research. Part C, Embryo Today: Reviews*, 84 (3), 245–256.

Curwin, B., and Bertke, S., 2011. Exposure characterization of metal oxide nanoparticles in the workplace. *Journal of Occupational and Environmental Hygiene*, 8 (10), 580–587.

Das, M., Saxena, N., and Dwivedi, P.D., 2009. Emerging trends of nanoparticles application in food technology: safety paradigms. *Nanotoxicology*, 3 (1), 10–18.

Dönmez Güngüneş, Ç., *et al.*, 2017. A comparative study on the in vitro cytotoxic responses of two mammalian cell types to fullerenes, carbon nanotubes and iron oxide nanoparticles. *Drug and Chemical Toxicology*, 40 (2), 215–227.

Ehrenberg, M.S., *et al.*, 2009. The influence of protein adsorption on nanoparticle association with cultured endothelial cells. *Biomaterials*, 30 (4), 603–610.

George, S., *et al.*, 2004. Fetal heart rate variability and brain stem injury after asphyxia in preterm fetal sheep. *American Journal of Physiology-Regulatory, Integrative and Comparative Physiology*, 287 (4), R925–R933.

Hamburger, V., and Hamilton, H.L., 1951. A series of normal stages in the development of the chick embryo. *Journal of Morphology*, 88 (1), 49–92.

Hanini, A., *et al.*, 2011. Evaluation of iron oxide nanoparticle biocompatibility. *International Journal of Nanomedicine*, 6, 787.

Hussain, S., *et al.*, 2005. In vitro toxicity of nanoparticles in BRL 3A rat liver cells. *Toxicology in Vitro*, 19 (7), 975–983.

Jae-Hyun, L., *et al.*, 2007. Artificially engineered magnetic nanoparticles for ultra-sensitive molecular imaging. *Nature Medicine*, 13, 95.

Jeng, H.A., and Swanson, J., 2006. Toxicity of metal oxide nanoparticles in mammalian cells. *Journal of Environmental Science and Health Part A*, 41 (12), 2699–2711.

Karlsson, H.L., *et al*., 2008. Copper oxide nanoparticles are highly toxic: a comparison between metal oxide nanoparticles and carbon nanotubes. *Chemical Research in Toxicology*, 21 (9), 1726–1732.

Karlsson, H.L., *et al*., 2009. Size-dependent toxicity of metal oxide particles – a comparison between nano- and micrometer size. *Toxicology Letters*, 188 (2), 112–118.

Ke, Y. and Qian, Z.M., 2003. Iron misregulation in the brain: a primary cause of neurodegenerative disorders. *The Lancet Neurology*, 2 (4), 246–253.

Kumari, M., *et al*., 2012. Repeated oral dose toxicity of iron oxide nanoparticles: biochemical and histopathological alterations in different tissues of rats. *Journal of Nanoscience and Nanotechnology*, 12 (3), 2149–2159.

Kumari, M., *et al*., 2013. Biochemical alterations induced by acute oral doses of iron oxide nanoparticles in Wistar rats. *Drug and Chemical Toxicology*, 36 (3), 296–305.

Lynch, I. and Dawson, K.A., 2008. Protein-nanoparticle interactions. *Nano Today*, 3 (1-2), 40–47.

Nations, S., *et al*., 2011. Acute effects of Fe_2O_3, TiO_2, ZnO and CuO nanomaterials on Xenopus laevis. *Chemosphere*, 83 (8), 1053–1061.

Noori, A., *et al*., 2011. Effect of magnetic iron oxide nanoparticles on pregnancy and testicular development of mice. *African Journal of Biotechnology*, 10, 1221–1227.

Pankhurst, Q.A., *et al*., 2003. Applications of magnetic nanoparticles in biomedicine. *Journal of Physics D: Applied Physics*, 36 (13), R167.

Patel, S., *et al*., 2016. DNA binding and dispersion activities of titanium dioxide nanoparticles with UV/vis spectrophotometry, fluorescence spectroscopy and physicochemical analysis at physiological temperature. *Journal of Molecular Liquids*, 213, 304–311.

Prasek, M., *et al*., 2013. Influence of nanoparticles of platinum on chicken embryo development and brain morphology. *Nanoscale Research Letters*, 8 (1), 251.

Rashidi, H., and Sottile, V., 2009. The chick embryo: hatching a model for contemporary biomedical research. *Bioessays: News and Reviews in Molecular, Cellular and Developmental Biology*, 31 (4), 459–465.

Sadiq, R., *et al*., 2015. In vitro toxicological assessment of iron oxide, aluminium oxide and copper nanoparticles in prokaryotic and eukaryotic cell types. *Drug and Chemical Toxicology*, 38 (2), 152–161.

Sawosz, E., *et al*., 2009. Nanoparticles of silver do not affect growth, development and DNA oxidative damage in chicken embryos. *Archiv Für Geflügelkunde*, 73, 208–213.

Singh, N., *et al*., 2012. The role of iron redox state in the genotoxicity of ultrafine superparamagnetic iron oxide nanoparticles. *Biomaterials*, 33 (1), 163–170.

Singh, N., *et al*., 2009. NanoGenotoxicology: the DNA damaging potential of engineered nanomaterials. *Biomaterials*, 30 (23-24), 3891–3914.

Skaper, S., *et al*., 1999. Excitotoxicity, oxidative stress, and the neuroprotective potential of melatonin. *Annals of the New York Academy of Sciences*, 890, 107–118.

Stohs, S.J. and Bagchi, D., 1995. Oxidative mechanisms in the toxicity of metal ions. *Free Radical Biology and Medicine*, 18 (2), 321–336.

Stroh, A., *et al*., 2004. Iron oxide particles for molecular magnetic resonance imaging cause transient oxidative stress in rat macrophages. *Free Radical Biology and Medicine*, 36 (8), 976–984.

Studnicka, A., *et al*., 2009. Influence of nanoparticles of silver/palladium alloy on chicken embryos' development. *Annals of Warsaw University of Life Sciences – SGGW Animal Science*, 46, 237–242.

Walkey, C.D. and Chan, W.C., 2012. Understanding and controlling the interaction of nanomaterials with proteins in a physiological environment. *Chemical Society Reviews*, 43 (27), 2780–2799.

Wang, J., *et al*., 2010. Pharmacokinetic parameters and tissue distribution of magnetic Fe(3)O(4) nanoparticles in mice. *International Journal of Nanomedicine*, 5, 861.

Zhu, X., Tian, S., and Cai, Z., 2012. Toxicity assessment of iron oxide nanoparticles in zebrafish (Danio rerio) early life stages. *PLoS One*, 7 (9), e46286